The Effect of PARP Inhibitor PJ34 on Metastatic Melanoma Cell Lines

Anna Marie Moe

This thesis is submitted in partial fulfilment of the requirements for the degree of Master in Medical Biology - Human physiology

Department of Biomedicine

University of Bergen

December 2016

Acknowledgements

First and foremost, I would like to thank my supervisor Professor Frits Thorsen for all his help and guidance. Thank you so much for making time to answer my many questions along the way. Also thank you for all your support and encouragement, especially in the times when the experiments did not work out as planned.

I would also like to thank Halala Sdik Saed and Bodil Berger Hansen for a lot of help in the lab and for teaching me several experimental techniques. Thanks to Tove D. Johansen for ordering my supplies whenever needed.

Great thanks to Endy Spriet and Hege Dale for all your help on the Nikon microscope. Thanks to Birth Berit Bergum for your great insight into the world of flow cytometry and helping me with the practical use of the flow cytometer and the FlowJo program.

Great thanks to PhD student Synnøve Nymark Aasen for help and encouragement along the way. Thanks to researcher Lars Prestegarden and post doc Kislay Roy for help in the lab.

I also want to thank former master students Billy and Nazanin for helping me at the very start of my masters and introducing me to the basic laboratory work. Thanks so much to all master- and medical students, PhDs and all the other employees at the 6.th floor of the BBB who made time to help me with occasional challenges.

I would also like to thank my family and closest friends for all their support. Especially thanks to my father for taking a strong interest in my project. Thank you for your willingness to discuss topics within molecular biology, despite your education and work within a completely different field. Finally, I would like to thank Kimmi for enduring all my technical questions regarding excel and other computer related topics. However, I wish to especially thank you for your tremendous support and encouragement throughout every single day.

Table of Contents

List of Figures

Abbreviations

Abbreviations	Full name
ADP	Adenosine diphosphate
Akt	Protein kinase B, a serine-threonine kinase. First identified as an oncogene from the AKT-8 thymoma cell line, derived from the AKR/J mouse
ATLV	Aggressive type of peripheral T-cell leukemia
ATM	Ataxia telangiectasia-mutated protein kinase
ATR	ATM and Rad3-related protein kinase
BBB	Blood-brain barrier
BCA	Bicinchoninic acid protein
BER	Base excision repair
BRAF	B-Raf proto-oncogene, a serine/threonine kinase
BRCA	Breast cancer gene
BSA	Bovine serum albumin
BTB	Blood-tumor barrier
Chk	Checkpoint kinase
CNS	Central nervous system
CTLA-4	Cytotoxic T-lymphocyte-associated antigen-4
Da	Dalton
DMEM	Dulbeccos modifies eagle medium
DMSO	Dimethyl suloxide
DNA	Deoxyribonucleic acid
DSB	Double stranded break
ECM	Extracellular matrix
EMT	Epithelial-mesenchymal transition
ERK	Extracellular signal-regulated kinases
EtOH	Ethanol/Ethyl alcohol
FA (pathway)	Fanconi anemia pathway
FCS	Fetal calf serum
FDA	Food and Drug Administration
FL2-A	Fluorescence parameter 2 - Area

FL2-H	Fluorescence parameter 2 - Height
FOXO3A	Forkhead box O3
FSC	Forward-scattered light, value measures cell size
GAPDH	Glyceraldehyde-3-Phosphate Dehydrogenase
GFP	Green fluorescent protein
GNAQ	Guanine nucleotide binding (G) protein, subunit alpha q
GNA11	Guanine nucleotide binding (G) protein, subunit alpha 11
G phase	Growth phase
HR	Homologous recombination
HRP	Horseradish peroxidase
HTLV	Human T-cell leukemia virus
IC_{50}	The half maximal inhibitory concentration
KIT	v-kit Hardy-Zuckerman 4 feline sarcoma viral oncogene homolog. A proto-oncogene tyrosine-protein kinase.
MAPK	Mitogen-activated protein kinase
MEK	MAPK/Erk kinase
Melanoma	Malignant melanoma of the skin
MET	Mesenchymal-epithelial transition
Milli Q	Autoclaved water
MMP	Matrix metalloproteinases
M phase	Mitotic phase
mTOR	Mammalian target of rapamycin
MW	Molecular weight
NOD/SCID	Nonobese-diabetic/severe combined immunodeficient mouse
NRAS	Neuroblastoma RAS viral oncogene homolog
ns	Not significant
NT	Neurotrophins
p-Akt (S473)	Phospolylation of Akt at serine 473
p-Akt (T308)	Phospolylation of Akt at threonine 308
PARP	Poly(ADP)-ribose polymerase
PBS	Dulbeccos phosphate buffered saline
PEN-STREP	Penicillin/Streptomycin
PI	Propidium Iodide

PI3K	Phosphoinositide 3 kinase
PJ34	2-(Dimethylamino)-N-(6-oxo-5,6-dihydrophenanthridin-2-yl)acetamide hydrochloride
PS	Phosphatidylserine
PTEN	Phosphatase and tensin homolog deleted on chromosome ten
PUVA	Psoralen plus ultraviolet A
p16	A tumor suppressor protein, also known as cyclin-dependent kinase inhibitor 2A
p53	A 53 kD nuclear phosphoprotein encoded by the proto-oncogene p53 (a tumor suppressor)
Rad51	Recombination Protein A
RAF	Rapidly Accelerated Fibrosarcoma, a serine threonine kinase
RAS	Family of retrovirus-associated DNA sequences. Gives small monomeric GTP binding proteins encoded by the ras gene
Resazurin	7-hydroxy-3H-phenoxazin-3-one 10-oxide
RNA	Ribonucleic acid
RNase	Ribonuclease
RPM	Rotation per minute
SD	Standard deviation
S phase	Synthesis phase
SSB	Single stranded break
SSC	Side-scattered light, value measures cell granularity
TBS	Tris-buffered saline
TBST	Tris-buffered saline with 0.1 % tween
UV	Ultra violet
VEGF	Vascular endothelial growth factor
WB	Western blot
WBTR	Whole-brain radiotherapy
WTS dye	Water-soluble tetrazolium salts dye

Abstract

Malignant melanoma is the most aggressive form of skin cancer. In addition, melanoma also has a high propensity to metastasize to the brain. Metastatic melanoma is generally associated with a poor prognosis. Brain metastasis is especially difficult to treat, in part due to the blood-brain barrier (BBB), making it difficult for anti-cancerous drug to reach the brain metastasis.

Several genes and signaling pathways are involved in the pathophysiology of melanoma, such as the MAPK pathway and the PI3K-AKT-pathway, which promotes survival, mobility and tumor cell growth. PARP1 has also been demonstrated to be upregulated in several cancers, including melanoma. PARP1 is involved in DNA repair, and attempts are being made to develop PARP inhibitors as therapeutics for cancers. PARP Inhibitor VIII (PJ34) is a potent PARP inhibitor, previously shown to cross an intact BBB. The main aim of this master thesis was to examine the effect of PJ34 *in vitro* on four different human metastatic melanoma cell lines. In addition, we also wanted to study potential *in vivo* effects of the drug.

Our work showed that PJ34 had a dose dependent inhibitory effect on cell viability on all four tumor cell lines used, both in 2D and 3D cell culture assays. The flow cytometry results suggested that PJ34 caused G_2M arrest and that PJ34 eradicated tumor cells through apoptosis. A dose-dependent inhibition of wound closure by the drug was also determined. Interestingly, it was also found by western blot (WB), that PJ34 actually increased the amount of PARP1. This might be due to an overcompensating mechanism in the treated cells. Moreover, PJ34 were found to inhibit phospho-Akt (Ser473) in two of the cell lines, suggesting that PJ34 may exert its effect through the PI3K-Akt pathway. PJ34 also inhibited growth of tumor spheroids. Although it have been demonstrated by others that PJ34 can inhibit cancer cells *in vivo*, our animal experiment did not show inhibition of tumor growth after treatment. WB performed on the *in vivo* tumors, showed an increase in PARP1 expression after treatment, similar as seen *in vitro*. In conclusion, we found that PJ34 effectively inhibits our metastatic melanoma cell lines *in vitro*. Our results also indicate that PJ34 is not a specific PARP1 inhibitor, but may act on other pathways such as the PI3K-Akt pathway.

1 Introduction

1.1 Incidence, Survival and Mortality of Malignant Melanoma.

Cutaneous malignant melanoma is the most aggressive form of skin cancer (1). However, it is also the least common type of skin cancer (2). Most patients with skin cancer have non-melanoma skin cancer. Non-melanoma skin cancer includes basal cell carcinoma and squamous cell carcinoma, which counts for 80% and 20% respectively, of all cases of non-melanoma skin cancer. Mortality is unusual for non-melanoma skin cancer (3). Malignant melanoma counts for less than 5 % of all skin cancer incidences, though, it is the cause of 75% of all skin cancer related deaths (3, 4). For simplicity, malignant melanoma will be referred to as merely melanoma from here on out. Moreover, one third of all cancers in the United States are in fact skin cancers (3). In 2012 melanoma occurred in 232 000 people and caused 55 000 deaths worldwide (5).

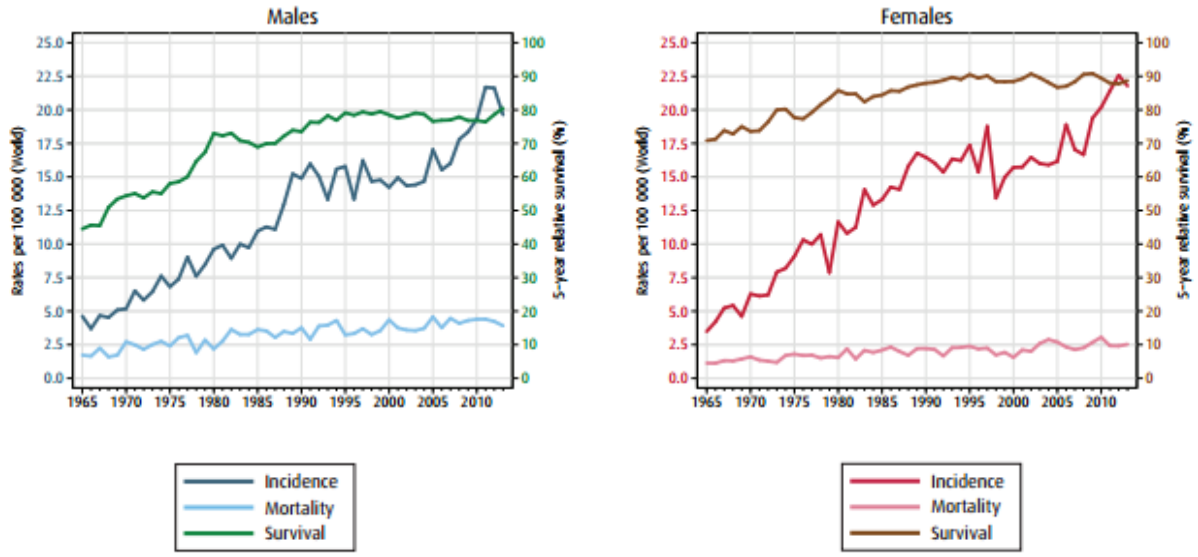

Figure 1.1 – Incidence, mortality and survival rates of melanoma of the skin: Data shown are from Norway in the period of 1965 – 2013. Incidence and mortality graphs correspond to the left y-axis (rates per 100 000), while the survival graph corresponds to the right y-axis (5-year relative survival in %). Graphs are from the Cancer Registry of Norway (6).

As we can see in figure 1.1, the incidence of melanoma in Norway per 100 000 has steadily increased in the last five decades. Incidence has been raised as much as around four times for males and six times for females. Even so, the mortality has only been doubled for both men and women. The 5 year survival rate has also increased for both (6). This is most likely due to earlier detection and better treatment of melanoma (7).

The incidence of melanoma in Norway is among the highest in the world (8). The incidence also increases significantly with age. However, melanoma is also one of the most common cancers found in adolescents and young adults. Especially in young women. For women ages 20 – 30 years, melanoma is the most common malignancy (4). Furthermore, the 5–year survival rate is high for localized melanoma, as we can see in figure 1.2. However, as the metastatic stages progresses the survival rate drops dramatically (9).

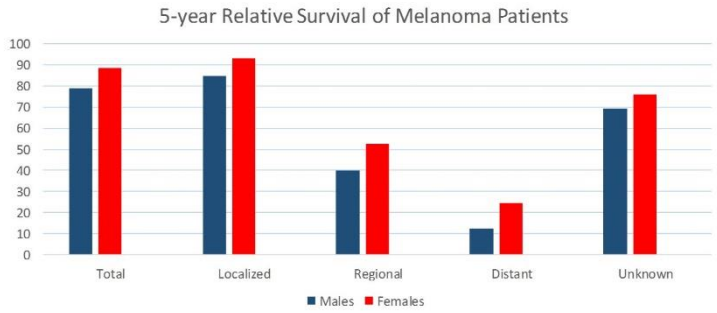

Figure 1.2 – The 5-year relative survival rate for melanoma patients: The data are from Norway for the time period 2009-2013 and they are divided into localized, regional and distant metastases. In addition, the numbers survival for unknown degree of metastases and the total survival rate are shown. All the survival rates are divided into male and female. The figure is based on data found in the Cancer Registry of Norway (9).

There is a prominent need for successful new therapies for patient suffering from metastatic melanoma. Attempts to improve the survival have generally failed. However, many new promising therapeutics are currently under investigation and the understanding of the biology of metastatic melanoma is increasing (10).

1.2 Causes and Risk Factors

The increase in melanoma incidence is most likely due to increased sun exposure, increased use of sun tanning beds and depletion of the protective ozone layer (3, 8). Ultra violet radiation (UV) is carcinogenic. The depth of transmission into the skin of the tree types of UV light is dependent of their wavelengths. UVC (wavelength 200-290 nm) only penetrates the superficial layer of the skin, UVB (wavelength 290-320 nm) penetrates the basal layer of the epidermis, and UVA (wavelength 320-380 nm) penetrates the dermis. UVB is most carcinogenic. The rings of the nitrogenous bases of DNA have conjugated double bonds, which absorbs UV radiation. UVB causes specific UV photoproducts; pyrimidine-pyrimidone photoproducts and cyclobutane pyrimidine dimers (11). In addition, early detection and

increase in classification of lesions as melanoma is partly the reason for increased incidence of melanoma (12, 13).

There are many exogenous (environmental) and endogenous risk factors that have been linked to melanoma (14). However, up to 65 % of melanomas are related to sun exposure. The total accumulated exposure to sun are suggested by some studies to be a very important risk factor (12). Melanoma risk is also higher in patients with a history of non-melanoma skin cancers and solar keratosis. These are both indicators of cumulative UV exposure (15). However, some studies suggest that long-term occupational sun exposure actually may be protective. Nevertheless, intermitted sun exposure is generally accepted as the most important factor (12). The history of sunburn, particularly sunburn at an early age has also been suggested by several epidemiological studies to increase the risk of melanoma (15).

Other risk factors for developing melanoma are pale skin, red or blond hair, many freckles and tendency to burn and tan poorly (16). In addition, having more than 50 acquired melanocytic nevi, more than five dysplastic nevi, large congenital nevi and nevi in general larger than 6 mm are risk factors for melanoma development (12). PUVA therapy (UV exposure), use of tanning beds and the rare autosomal recessive photodermatosis named xeroderma pigmentosum are also risk factors (2, 12, 14). Even more risk factors include scars, immunosuppression, chemical exposure and Marjolin's ulcer (12, 14). The genetic factor is also important, since 8 – 12% of melanomas occur in a familial setting (12). In 41 % of familial melanomas there are mutations in the p16 pathway, which is a regulator of the cell cycle (17).

1.3 Biological Aspects of Melanoma

Most often melanomas arise within epidermal melanocytes of the skin. However, melanoma can also arise from non-cutaneous melanocytes such as those lining the choroidea, the mucosal surfaces of the gastrointestinal and genitourinary tract or the meninges (18). These primary non-cutaneous melanomas account for less than 7% of all melanomas (19, 20). Melanocytes are specialized dendritic cells that originates from the neural crest. Melanocytes produce melanin and are mainly confined to the basal layer of the epidermis were they form a complex relationship with keratinocytes (2, 21). Melanosomes are the specific cytoplasmic

organelles within melanocytes, were melanin is synthesized. From there melanin is transported via dendrites to adjacent keratinocytes (14, 21).

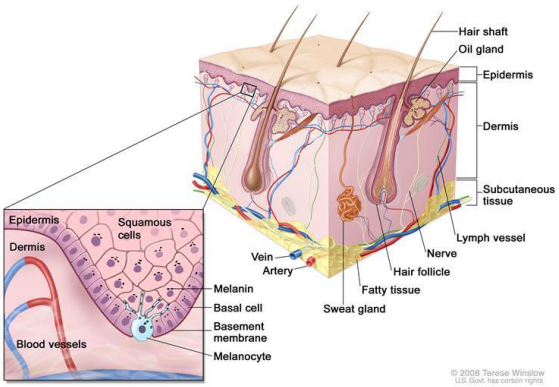

Figure 1.3 – Skin tissue: The image shows a schematic representation of normal skin tissue. Reprinted from National Cancer Institute (22).

Melanin can be synthesized as brown-black eumelanin or red-yellow phaeomelanin. The ratio of these mainly determines skin and hair color. The density of melanocytes is independent of ethnicity (21). It is rather the number, size and distribution of melanosomes within keratinocytes and the type of melanin, that the color depends on (2). Melanin formation in the skin is a natural defense mechanism against UV absorption, and it can be seen as tanning of the skin. To eliminate UV-damaged skin cells, apoptosis can be initiated in the cells. This can be seen as peeling of the skin after a sunburn (11). Furthermore, benign melanocytic nevi are most commonly referred to as moles (2). Acquired melanocytic nevi, dysplastic melanocytic nevi (atypical nevus) and congenital nevi (normally present at birth) are precursor lesions to malignant melanoma. The presence and increased number of these leads to increased risk of developing melanoma (23). However, most melanomas do not arise in pre-existing melanocytic nevi, but de novo (2).

1.4 Molecular Aspects of Melanoma

Several genes in signaling pathways involved in growth and proliferation are implemented in the pathophysiology of melanoma. Growth factor receptors reside on the surface of melanocytes, and they are stimulated by growth factors or other ligands that trigger cell division and proliferation. Several growth factors acts through tyrosine kinases. They will again trigger signaling cascades that activate signals for proliferation and survival, like BRAF, NRAS and PI3K. In addition, there are also several breaks for proliferation, like p16,

and damage checkpoints, like p53. These genes can be mutated to allow growth and proliferation to continue without the normal regulation from them. Genetic mutations called "driver mutations" will actively promote cancerous behavior, while "passenger mutations" does not actively contribute to oncogenic behavior, but may still suggest carcinogenic exposure of the cells (17). Some of the repeated "driver mutation" in melanoma includes BRAF, GNA11, GNAQ, KIT, MEK1 (MAP2K1) and NRAS, which induce and sustain tumorigenesis (24). The understanding of the genomics behind melanoma development has been very important in the development of personalized medicine. Therapies are developed to target driver mutations in melanoma development (17).

In human melanoma there are frequent genetic alterations in components in the mitogen-activated protein kinase pathway (MAPK: RAS-RAF-MEK-ERK), which play an important role in melanoma proliferation, differentiation, survival, invasion and angiogenesis (17, 25, 26). Consequently the MAPK pathway is often activated in melanomas (26).Two essential genes in the MAPK pathway is BRAF and NRAS. Around 70 % of all melanomas harbor a mutation in one of these two genes, especially in BRAF (25). BRAF encodes a serine/threonine protein kinase, which is a prominent regulator of the MAPK signaling pathway. In cutaneous melanomas, more than 60% harbor a BRAF-mutation (17). Furthermore, more than 80% of these BRAF mutations feature the specific V600E valine to glutamic acid substitution mutation (17, 26). The serine threonine kinase inhibitor, Vemurafenib has in recent years been approved by the US Food and Drug Administration (FDA) for treatment of $BRAF^{V600E}$ mutated melanomas (26).

The PI3K-AKT-mTOR pathway is also an essential cellular signaling pathway, which promotes survival, mobility and growth (17, 27). Similar to the MAPK pathway, PI3K is also often activated in melanoma (26). However, it has not yet been found any mutations in PI3K in melanoma. In spite of this, the downstream component Akt3 and the negative regulator of PI3K, namely PTEN, have been implicated in melanoma (17). PTEN is a negative regulator of Akt, and by preventing phosphorylation of Akt it inhibits the PI3K pathway (26). In 43-60% of melanomas, mutations that activate Akt family members are found (17). Rad51 recombinase is important in repair of double stranded breaks (DSBs) and homologous

recombination (HR). Overexpression of Rad51 is found in many human tumor cells, among others, melanoma. This overexpression can lead to increased resistance to DNA damage and contribute to chemotherapeutic drug resistance in these tumors. In addition, overexpression of Rad51 can lead to increased instability of the genome as well as contributing to carcinogenesis (28).

1.5 Stages of Melanoma

The different stages of melanoma progression, are determined by the thickness, ulceration and the degree of spreading to lymph nodes and distant parts of the body (29). The patient's prognosis is strongly influenced by the degree of progression of the melanoma at the time of diagnosis. Melanoma detected early is most often cured. Though, as tumor thickness and the disease stage increase, survival rates steadily declines (30, 31). The different stages of melanoma are portrayed in figure 1.4. In stage 0, also called melanoma in situ, abnormal melanocytes in form of a tumor in the epidermis are found. These melanocytes can become cancerous and invade nearby tissue (29, 32). In Stage 1 and 2 melanoma is still confined to the skin, but have now reached the dermis (second layer of the skin) or further. In stage 3 the cancerous melanocytes have spread to the nearby lymph nodes. In stage 4 melanoma has spread to other parts of the body such as the distant lymph nodes and skin, as well as liver and the lungs (32).

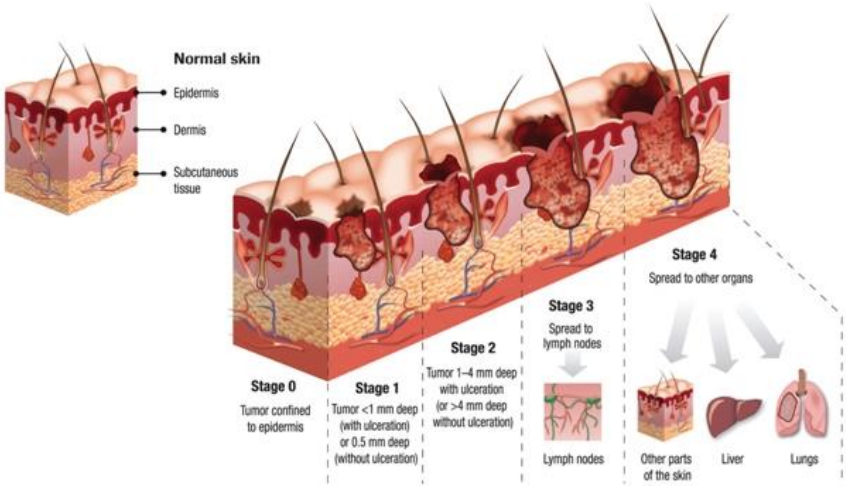

Figure 1.4 – Stages of cutaneous melanoma: Figure is reprinted from (32).

1.6 The Metastatic Process with Focus on Spreading to the Brain

The spread of malignant cells from a primary tumor to distant sites of the body is called metastasis. This is the largest problem within cancer treatment and it is the main cause of death for cancer patients. Metastasis occurs in a series of steps called the "invasion-metastases cascade" (33).

Epithelial-mesenchymal-transition (EMT) has been shown to play a key role in metastasis in epithelium-derived carcinoma. It starts with activation of the EMT program in the cancerous cells and local invasion. To accomplish this, the epithelial tumor cell has to acquire motility and degrade the underlying base membrane and the extracellular matrix (ECM). The second step consist of intravasation by the cancer cells, were the cells penetrate nearby blood- or lymphatic vessels. Once in the systemic circulation, the cells are transported through the circulatory system (step three), however, only a few cells seem to be able to survive in the circulation. The fourth step is the escape of cancer cells from the vascular lumen and into the parenchyma in distant tissues, called extravasation. The fifth and final step is the colonization, with the growth of micrometastasis that can lead to macroscopic secondary tumors. The colonization of macroscopic tumors, require reversion of EMT and/or activation of mesenchymal-epithelial transition (MET) (34, 35). To metastasize successfully, there is a need for contribution of the microenvironment like ongoing ECM remodeling and angiogenesis. Furthermore, recent evidence suggests that long range signals can be released by primary tumors that prepare a future site for metastasis. Thus, the future site is then called a pre-metastatic niche (11, 33).

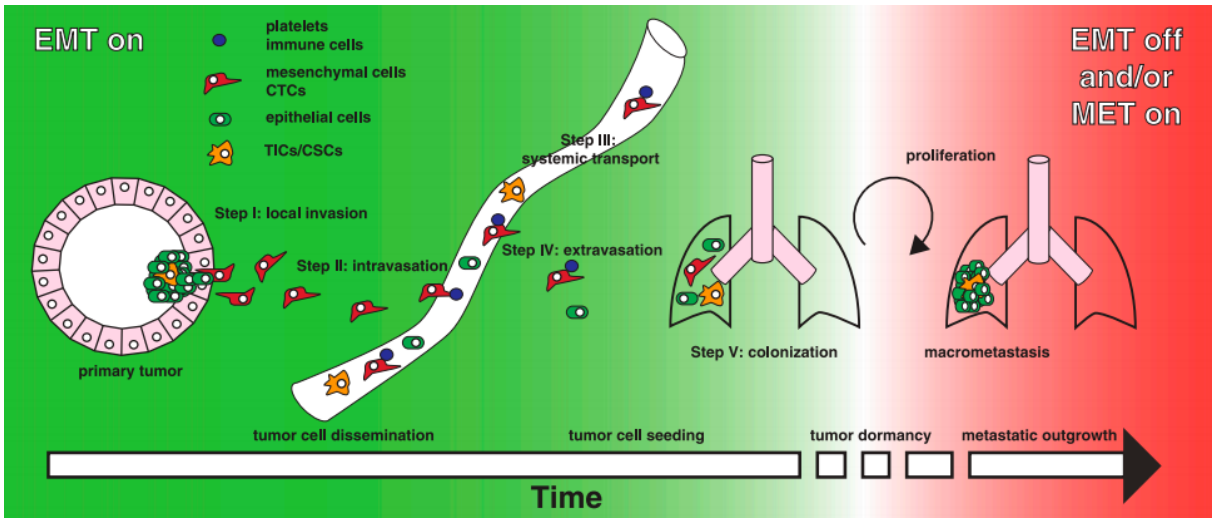

Figure 1.5 – The metastatic process: The figure shows the different steps of the "invasion metastases cascade" as well as the reversibility of EMT over time. Reprinted from (34)

If a cancerous cell is to form a successful metastases in the brain, through the blood vessels, every step of the metastatic cascade has to be completed. The local invasion of the brain is dependent on cell motility, adhesion and enzymatic remodeling of the ECM. Paracrine interactions between brain stromal and endothelial cells and the invading cancerous cells are necessary for brain invasion. After entering the brain parenchyma, the metastatic cancer cells has to adhere to the substratum in order to survive (36).

Primary tumors can have characteristics that predispose them to spread through blood vessels. High interstitial pressure, an immature neovascular system and close proximity of blood vessels to the cancer cells, can encourage intravasation. Primary tumors contain subpopulations of cells that possess different degrees of metastatic potential. The brain is unique as a target for metastases, as it lacks lymphatic drainage and is surrounded by the blood-brain barrier (BBB). The brain has a special microenvironment; it is drained in interstitial fluid, which is high in chloride. When it comes to different kinds of metastatic cells from epithelial origin, this environment may not be conductive (36). However, it can be that this unique environment attract cells from neuroepithelial origin, like melanoma. Melanoma and neurons share the same embryonal origin (derived from the neural crest). Consequently, the frequent involvement of CNS metastases in melanoma may be due to a so-called "homing" phenomenon (36, 37).

Molecular factors important in brain metastases include, among others, neurotrophins (NTs), matrix metalloproteases (MMPs) and vascular endothelial growth factor (VEGF) (36-38). NTs are notable because they stimulate brain invasion. NTs have been found to promote invasion in brain metastatic melanoma cells, by enhancement of the production of enzymes that locally can degrade the EMC and the BBB membrane. Degradation of EMC is believed to assist invasion by clearing a pathway for the cancerous cells. MMPs also have the ability to degrade the ECM, by breakdown of connective tissue barriers. MMPs correlate with invasiveness, metastasis and a poor prognosis in several metastatic tumors. In addition, MMPs have been found to be upregulated in brain metastases. Moreover, VEGF is reported to be involved in angiogenesis and growth of brain metastasis. Upregulating of VEGF may also contribute to the ability of some cancers to form brain metastasis (36). The new vessels induced to form by VEGF does not hold all the same properties as those normally found in

the brain. These new vessels can in turn cause increased leakage trough the blood-brain barrier (39).

1.7 Brain Metastases and the Brain Blood Barrier

Brain metastases commonly originates from the following primary cancers; lung cancer (50%), breast cancer (15 – 20%), melanoma (10%) and colon cancer (5%) (40). These statistics are portrayed in figure 1.6. In more than 70 % of the cases, metastases to the brain are multiple. However, solitary metastases also occur (41). Brain metastasis are also much more common than primary brain tumors and outnumber them by at least 10 to 1. In as much as 20 – 40% of cancer patients brain metastasis occur (41, 42).

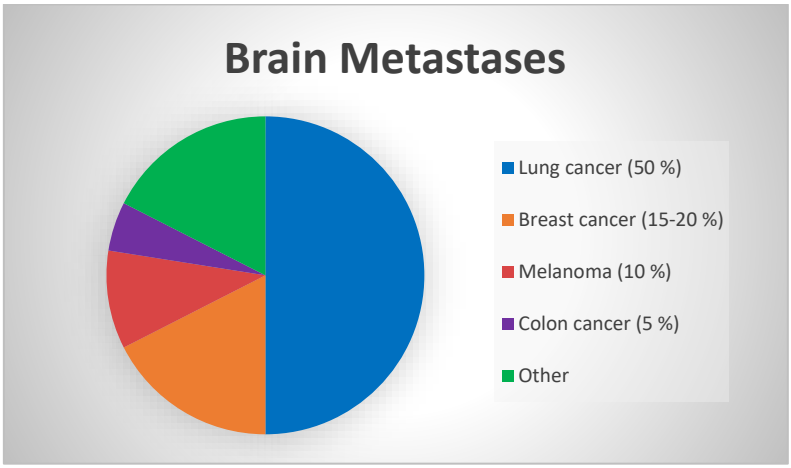

Figure 1.6 – Brain metastases: The figure shows a pie chart of the different primary cancers that brain metastases originates from in percent. The chart is created based on data from (40).

Of all cancer types, melanoma has the highest propensity to metastasize to the brain. Patients with advanced melanoma have approximately a 50% chance of developing brain metastases. In addition, improved detection methods and improved cancer treatment in general (which cause prolonged survival) seems to cause a rise in the incidence of brain metastases (7). Considerable advancements have been made in diagnosis and treatment of brain metastases that has improved patient survival and life quality. However, diagnosis of brain metastases still generally indicate a poor prognosis (42). In a large study concerning melanoma patients with brain metastases, the median survival was merely 3.8 months (7).

The blood-brain barrier (BBB) is formed by capillary endothelium in the brain (43). The BBB consists of continuous epithelium with tight junctions and no fenestrations. In addition, the

terminal processes of astrocytes cover the BBB and help keep its integrity (39). The BBB excludes all large neurotherapeutic molecules, and over 98 % of small drug molecules (43). The expression of an active drug efflux pump in the BBB, also contributes to the limitations of the drug uptake (26, 39). In addition to the BBB, the lack of lymphatic vessels also prevent most drugs and microorganisms to enter the brain (39). If brain tumors exist, the BBB in this area is often referred to as the blood-tumor barrier (BTB). An intact BTB limits the anti-cancerous drug delivery to the brain metastases (7). However, the permeability of the BBB increases at the later stages of brain metastases. Drugs with small molecular weight (MW), such as vemurafenib are suggested to potentially be able to cross the BBB in early stages of brain metastases (26). Generally small molecules can cross the BBB if the MW is less than 400-500 Da and if it is lipid soluble (43).

1.8 Treatment of Metastatic Melanoma

For patients with metastatic melanoma the 10-year survival rate is less than 10%. Systemic therapy is the main part of treatment for most patients with metastatic disease. This includes cytotoxic chemotherapy, immunotherapy or a combination such as biochemotherapy. However, surgery and radiation therapy also play a role. There is a very high need for successful new therapies for metastatic melanoma. Attempts to improve survival for patients with metastatic disease have generally failed. However, many new promising therapeutics are currently under investigation, and the understanding of the biology of metastatic melanoma is increasing (10).

Brain metastases are common in advanced melanoma patients, and treatment of brain metastases usually rely on surgery or radiotherapy in addition to chemotherapy (44). Chemotherapy alone is generally not successful in treating brain metastases from metastatic melanoma (44, 45). However, Temozolomide has been the most promising drug treatment (7). Furthermore, the other conventional treatments also have limited success, like radiotherapy with our without previous surgical resection. Radiotherapy can be global treatment, like whole-brain radiotherapy (WBRT) or local treatment like stereotactic radiosurgery. The reasons for the limitations of these treatments are due to the fact that melanoma is often radio-resistant and that multiple brain metastases often occur (26, 45).

Nonetheless, in 2011 two new treatments for advanced melanoma were approved by the US FDA. Ipilimumab (Yervoy™) is one of these drugs. Ipilimumab increases cellular immunity and reduces the tolerance to tumor-associated antigens and thereby increases activation of an immune response against the metastatic melanoma cells. Ipilimumab exerts its effects through acting as a monoclonal antibody against the cytotoxic T-lymphocyte-associated antigen-4 (CTLA-4) receptor. The other FDA approved drug is Vemurafenib (Zelboraf®). As mentioned in subchapter 1.4, Vemurafenib can be used to treat $BRAF^{V600E}$ mutated malignant melanomas, and by inhibiting mutated BRAF it can correct the abnormal activation of the MAPK pathway (26, 45). These two therapeutic compounds may be a viable alternative for management of metastatic melanoma in the brain (45). Though definite data are presently lacking, Vemurafenib has shown encouraging result in clinical trials regarding advanced melanoma (26, 45).

1.9 PARP1

Poly(ADP)-ribose polymerase 1 (PARP1) is a nuclear protein who plays a key role in DNA repair and is also involved in pathways related to formation of tumors (46, 47). DNA damage activates PARP1, which facilitates single stranded-break (SSB) repair, through the base excision repair (BER) pathway (47-49). Moreover, PARP1 expression has been found to be upregulated in several cancers, including melanoma (47).

The current attempts to develop PARP inhibitors as therapeutic drugs for cancer, is based on over 40 years of research (50). PARP inhibitors were designed to block the catalytic activity of the PARP enzyme and also to resemble the by-product nicotinamide (51). One reason for the antitumor effects of PARP inhibitors is their ability to induce synthetic lethality in cells who have deficient homologous recombination repair (HRR), e.g. loss-of-function mutations in the tumor suppressor genes BRCA1 and 2 (27, 46, 47). Inhibition of PARP1 leads to accumulation of unrepaired SSB, which results in replication forks arrest. This arrest cause DNA double stranded breaks (DSBs) and DSBs are normally repaired by HR. However, if the tumor cells have deficient HRR due to BRCA mutations this repair will be impaired. This explains why tumors with defective BRCA are hypersensitive to PARP inhibitors (27, 49, 52-54).

Olaparib was in 2014 the first PARP inhibitor that was approved by the European Medicines Agency to be used for maintenance therapy for patients with BRCA1/2-mutant ovarian cancer, following chemotherapy (48). In addition to synthetic lethality in HR deficient tumors, PARP inhibitor may synergize with cytotoxic drug or ionizing radiation that cause DNA damage (49). Moreover, PARP1 itself is also involved in repair of DSB through the HR pathway, however PARP1 is not required for HRR (55, 56). A PARP1 defect is not associated with accumulation of mutations and cancer. This may be because cells lacking in PARP1 or subjected to PARP1 inhibition, indeed have an increase in homologous recombination (HR) (56). Rad51 recombinase is an important factor for HR and repair of DNA DSBs (28). This may suggest Rad51 as a potential target to combine with PARP1 inhibitors. The PI3K-Akt pathway also interacts with DNA damage response. As previously mentioned, activation of this pathway, promotes proliferation, mobility, growth and survival, and is common in many tumors (17, 27, 53). The combination of PI3K inhibitor with PARP inhibitor as a therapeutic strategy against cancer has been discussed. Previous studies have shown that inhibition of PI3K signaling can increase the effects of PARP inhibitors in the eradication of cancer cells (27).

1.10 PARP Inhibitor VIII (PJ34)

PARP Inhibitor VIII (PJ34) is an inhibitor of poly(ADP-ribose) polymerase 1 (PARP1) (57, 58). It is also a cell-permeable and water-soluble phenanthridinone derivative (59). PJ34 were discovered in 2001, and since then it has been used at rather high micromolar (μM) concentrations in over 150 publications involving PARP biology (60). The reason for using PJ34 in these publications was its high affinity for PARP1, its water solubility and cellular residence time. There have been a very limited knowledge about PJ34s target profile in these publications and usually it was taken for granted that PJ34 was a highly potent selective PARP1 inhibitor. Only recently, an extensive profiling of PJ34 across 13 members of the human PARP family has been performed. That PJ34 is a high affinity inhibitor of PARP1 was confirmed in the study. However, the study also revealed affinities to PARP2, TNKS1, PARP3, PARP4 and TNKS2. In addition, residual affinities to PARP14, PARP15 and PARP16 were shown. A weak affinity to the matrix metalloproteinase MMP2, which is not a part of the PARP family, has also been reported. PJ34 also seems to have some unique properties relative to other PARP inhibitors, which suggests that factors independent of PARP1, not yet identified, also may be responsible of the observed effects of PJ34 (60).

PJ34 was originally designed to protect cells from apoptotic cell death induced by high PARP1 activity in response to DNA damage caused by stroke, brain injury, myocardial infraction or inflammation (61, 62). However, PJ34 has been reported to enhance chemotherapeutic effects in certain tumor types (57). In addition, PJ34 alone has been shown to cause growth inhibition, cell cycle arrest and apoptosis in cancer cells (58, 63). Furthermore, as mentioned, if a drug is to cross the BBB to treat brain metastases, the molecular weight has to be below 400 – 500 Da (43). PJ34, has a molecular weight of 331.8 Da, and previous studies show that PJ34 is able to cross an intact BBB (59, 64).

1.11 Experimental Methods

Several cell lines for both basic and applied research has been produced by disaggregated cancer tissue. Furthermore, existing preclinical research depends heavily on monolayer cultured cells (65). Our understanding of the biological mechanism behind cellular functions, e.g. migration and differentiation, rely mainly on results from studying cell in two dimensional (2D) cultures (66). This is in spite of the considerable amount of evidence showing that three dimensional models are superior to two dimensional assays (65). The 3D culture assays bridge the gap between cell culture and live tissue (67).

Further in this chapter, basic principles behind some of the *in vitro* assays used in this thesis, will briefly be explained.

1.11.1 Cell Viability

In the cell viability assays, resazurin dye (7-hydroxy-3H-phenoxazin-3-one 10-oxide), also called Almar Blue was used as an indicator of cell viability. Resazurin has been used in several proliferation and cytotoxicity assays to determine cell viability. There is a direct correlation between the reduction of resazurin to resorufin and the number of live organisms, such as e.g. mammalian cells. By the use of a spectrophotometer the absorbance of resazurin and resorufin can be measured (68). The magnitude of the dye reduction correlates with the number of viable cells (69).

1.11.2 Flow Cytometry

The measurement of cells in a flow system is called flow cytometry. The cells pass a point of measurement with focused light one at a time, see figure 1.7. The flow cytometer then records the scattered light and different wavelengths of fluorescence. Fluorescent chemicals can be used to label components of the cell, like DNA. Another method is the attachment of antibodies to several cellular proteins. The fact that flow cytometric analyses requires a suspension of single cells is a major disadvantage, because then tissue architecture and information about the spatial relationship are lost (70).

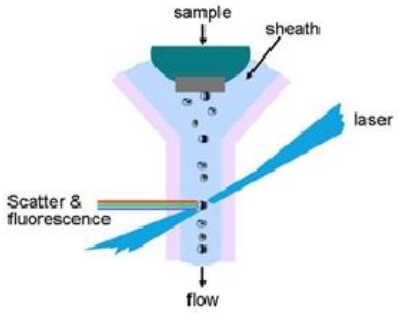

Figure 1.7 – Flow chamber: This figure shows the basic feature of a flow chamber (70).

DNA analysis is an important application of flow cytometry. The distribution of cells throughout the cell cycle can be determined by measuring the DNA content of the individual cells, see figure 1.8. The most common fluorescent dye to measure the DNA content is propidium iodide (PI). PI binds to DNA and has red fluorescence, which can be excited at 488 nm. PI stains all double stranded nucleic acids, and therefore the cells have to be incubated with RNase, to remove double stranded RNA, before analysis. In addition, PI is excluded by the plasma membrane, and therefore rely on fixation or permeabilization prior to adding the dye (70).

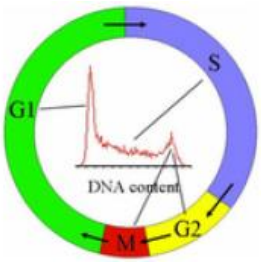

Figure 1.8 – The relationship between the DNA histogram and the cell cycle: Though this figure does not show cells in the G_0 phase, which is technically out of the cell cycle, G_0 has the same DNA content as the cells in G_1. Figure reprinted from (70).

The lack of membrane integrity is usually what defines necrotic cells. This can also be measured by flow cytometry. In contrast, apoptotic cells have an intact plasma membrane. Necrotic and apoptotic cells *in vivo* will normally be removed by phagocytosis. *In vitro*, the apoptotic cells will in the end lose their membrane integrity, which can be referred to as secondary necrosis. However, there are several distinctions between necrosis and apoptosis. Most importantly, necrosis is a disordered process, while apoptosis is a structured and orderly process specifically designed to remove unwanted cells (70). Annexin V can be used to detect apoptotic cells by flow cytometry. Phosphatidylserine (PS) residues are normally hidden on the inside of the plasma membrane. In early apoptosis PS residues appear on the cell surface, due to translocalization from the cytoplasmic face. The expression of PS on the surface of the cells holds a key role in macrophage recognition and removal of apoptotic cells. As Annexin V has a strong, Ca^{2+}-dependent, affinity for PS it can be used to detect apoptotic cells (71, 72).

1.11.3 Western Blotting

To identify and separate proteins, western blotting can be utilized. Different proteins in a mixture are separated based on molecular weight (MW) through gel electrophoresis. When the proteins are loaded onto the gel they have a negative charge, due to denaturing by heating. When voltage is applied, the proteins will thus travel toward the positive electrode. The results from the gel electrophorese is thereafter transferred to a membrane, which will show a band for each protein. To identify the protein of interest, the membrane is incubated with label antibodies specific to current protein. Antibodies which are not bound are washed off and the bound antibodies are detected by developing the film, usually in a dark room. The label antibody is usually detected with an enzyme, like horseradish peroxidase (HRP), which is detected by the signal it produces that is corresponding to the position of the protein of interest. Only the band from the protein of interest should then be visible. The band thickness and intensity corresponds to the amount of protein present. It is important to note that western blotting results are usually considered to be semi-quantitative. The western blot does not provide an absolute measure of quantity, however, it still gives us a relative comparisons of protein levels (73).

2 Aims

The main aim of this master thesis was to examine the effect of the PARP inhibitor PJ34 *in vitro* on four different human metastatic melanoma cell lines. Another main aim was to determine potential *in vivo* effects of the drug.

Six sub aims were defined within the work of this master thesis:

1. To use monolayer- and soft agar assay to study the effect the drug has on cell viability.
2. To employ flow cytometry to study the effects of the drug on cell cycle and apoptosis.
3. To examine the drug effect on migration by the use of scratch wound assay.
4. To use western blot to study the effect of the drug on different proteins, mainly PARP1 expression.
5. To examine the drug effect on tumor spheroids.
6. To determine the effect of the drug on subcutaneous tumors *in vivo.*

3 Materials and Methods

3.1 General Cell Culture Techniques

3.1.1 Cell Lines Used: H1_DL2, H3, Melmet 1 pGF1 and Melmet 5 pGF1

In this master project four different metastatic cell lines, derived from malignant melanoma, were used. They were H1_DL2, H3, Melmet 1 pGF1 and Melmet 5 pGF1. Both the H1 and H3 cell lines were developed in our laboratory from resected tumors of two patients with melanoma brain metastases. (26, 74). To obtain the H1_DL2 cell line the H1 cells were transduced with a green fluorescent protein (GFP) and luciferase. Before the tumor material was collected, written consents were obtained from the patients (26). Melmet 1 pGF1 originated from subcutaneous melanoma tissue and Melmet 5 pGF1 were derived from a melanoma lymph node metastasis. Both these cell lines were also transduced with green fluorescent protein (GFP) and they were a kind gift from Prof. Øystein Fodstad at the Oslo University Hospital (75).

3.1.2 Passaging

Table 3.1: Some equipment used for general cell culture techniques.

NAME	SUPPLIER
ALT DMEM:	
450 mL Dulbeccos Modified Eagles Medium	Sigma-Aldrich Inc., MO, USA
50 mL Heat inactivated fetal calf serum (FCS)	Fisher Scientific, MA, USA
10 mL L-Glutamine, 200 nM	BioWhittaker, Verviers, Belgium
10 mL Penicillin/Streptomycin (PEN-STREP), 100 µL/mL	BioWhittaker, Verviers, Belgium
16 mL Non essential amino acids 100X	BioWhittaker, Verviers, Belgium
0.1 mL Plasmocin, 25 mg/mL	Invivogen, CA, USA
*Dulbeccos phosphate-buffered saline 10X	Sigma-Aldrich Inc., MO, USA
Trypsin EDTA, 0.25%	BioWhittaker, Verviers, Belgium
100 % dimethyl sulphoxide (DMSO)	Sigma-Aldrich Inc., MO, USA
Blue filter cap sterile culture flasks: 25 cm^2, 75 cm^2 and 175 cm^2	Thermo Scientific, Nunc, Roskilde, Denmark
Sterile and disposable pipettes: 5, 10 and 25 mL	Corning Incorporated, NY, USA

*All of the PBS used in this master thesis is made from Dulbeccos phosphate-buffered saline 10X (Sigma-Aldrich Inc., MO, USA) (see table 3.1) diluted with autoclaved milliQ water. 50 mL Dulbeccos phosphate-buffered saline 10X was added to 450 mL autoclaved milliQ water.

All the cell lines were kept in culture flasks (Nunc As, Roskilde, Denmark) in a 5% CO_2 incubator at a 100 % humidity and 37°C. ALT DMEM (see table 3.1) was used as growth medium and the cell lines were cultured in monolayer. The cells were passaged regularly, normally when reaching a confluence between 70-80%. The cells were discarded after 10-15 passages. The cells were normally kept in large (175 cm^2) culture flask with blue filter caps (see table 3.1). However, at some occasions 75 cm^2 and 25 cm^2 culture flasks were used (see table 3.1). When passaging a large (175 cm^2) culture flask, all liquid was first removed from the flask, the cells were washed with 6-8 mL of PBS and 4 mL of trypsin EDTA was added (see table 3.1). When the cells had detached from the bottom of the flask (usually after 5 minutes in the incubator) 5 mL of ALT DMEM were added to the culture flask to neutralize the trypsin, and the cell solution was resuspended. Part of the cell solution was transferred to a new large culture flask. The amount of cell solution transferred depended on how fast the particular cell line grew, when the next experiment would be performed and how much of the cell line were needed. ALT DMEM was added to make a total volume of 35 mL.

3.1.3 Freezing and Thawing Cells

Freezing was normally done when the large (175 cm^2) culture flask was 70-80% confluent. First, a normal passaging procedure was followed (see subchapter 3.1.2.). After retrieving a resuspended cell solution consisting of 5 mL ALT DMEM, 4 mL Trypsin EDTA and cells, this cell solution was transferred to a sterile conical 15 mL centrifuge tube (Thermo, Scientific, Nunc, NY, USA). The 15 mL tube was centrifuged at 900 rpm for 4 minutes. The supernatant was removed and 4 mL of freezing solution was added to the 15 mL tube and resuspended. The freezing solution consisted of a 1:1 mix of two other solutions. The first of the two, consisted of 4.5 mL ALT DMEM and 0.5 mL Fetal Calf Serum mixed together. The other solution consisted of 1 mL 100% DMSO and 4 mL PBS. The resuspended freezing solution with cells were then pipetted into four 1 mL cryotubes (Thermo Scientific, Nunc, Roskilde, Denmark). The cryotubes were kept in a -80°C freezer for one day and afterwards transferred to a liquid nitrogen tank (Thermo Scientific, Iowa, USA) for long term storage. When more cells were needed, the cryotubes were taken out of the nitrogen tank and placed in a water bath set to a temperature of 37°C to thaw. Afterwards, the cell solution was pipetted directly into a 25 cm^2 culture flask. 10 mL ALT DMEM was added and resuspended with the cell solution.

3.2 Experimental Preparations

3.2.1 Drug used: PARP Inhibitor VIII (PJ34)

Table 3.2: PARP Inhibitor VIII, PJ34: Information is adopted from webpage (59).

PARP Inhibitor VIII (PJ34)	
Synonym:	2-(Dimethylamino)-N-(6-oxo-5,6-dihydrophenanthridin-2-yl)acetamide hydrochloride
Application:	A potent and cell-permeable inhibitor of PARP
CAS Number:	344458-15-7
Purity:	≥ 98%
Molecular weight:	331.8(Da)
Molecular formula:	$C_{17}H_{17}N_3O_2$•HCl
Appearance:	Powder
Physical state:	Solid
Solubility:	Soluble in water (22mg/ml), and DMSO (100mM)
Storage:	-20°C

Table 3.2 shows some important information about the drug used in this thesis, namely PARP Inhibitor VIII, PJ34 (Santa Cruz Biotechnology, Dallas, Texas, USA). The drug came as powder and was stored at -20°C. A stock solution (100 mM) was made by dissolving PJ34 in DMSO. The resulting stock was divided into smaller portions in 0.5 mL autoclaved Eppendorf tubes (Eppendorf AG, Hamburg, Germany) and frozen again at -20°C. When making drug concentrations before experiments, the stock was warmed up by hand. The stock was then diluted with ALT DMEM to the appropriate concentrations.

3.2.2 Counting of Cells

The cells were counted prior to performing *in vitro* experiments. After trypsination of the cells, ALT DMEM was added and the cell solution resuspended, and 10 uL of the cell solution were transferred to a 0.5 mL sterile Eppendorf tube (Eppendorf AG, Hamburg, Germany). Afterwards, 10 µL of 0.4% Trypan blue stain (Life Technologies, OR, US) was added to the tube in order to stain dead cell nuclei. 10 µL of the solution was then transferred to each side of a cell counting chamber slide (countess ™, Invitrogen, Oregon, USA) and inserted into the Countess™ Automated Cell Counter (Invitrogen, Oregon, USA). The focus of the image was adjusted according to the users guidelines. The total number of cells/mL and the number of live- and dead cells/mL were determined by the cell counter. The mean value from two individual counting's of live cells/mL was used to calculate the mean number of cells/mL in the cell solution. Based on this, the required amount of cells for each *in vitro*

experiment could be calculated. The corresponding amount of cell solution was transferred into a new 15 mL tube and ALT DMEM was added to obtain the desired number of cells/mL.

3.3 Cell Viability Assays

3.3.1 Monolayer Proliferation Assay

In the monolayer proliferation assay, 96-well plates were used (Thermo Scientific, Nunc, Roskilde, Denmark). 5 000 cells in 100 µL medium were pipetted into each well of the 96-well plate by the use of an eight-armed pipette and disposable pre sterilized ART® 200 pipette tips (Molcular BioProducts, Inc., San Diego, CA, USA). Afterwards, the 96-well plates were incubated for 24 hours to make sure the cells were attached to the surface. Drug was added to the 96-well plate in concentrations of: 0.001 – 0.01 – 0.1 – 0.5 – 5 – 50 – 100 µM. Each of the concentrations was added to a whole column (8 repetitions) in the plate. 100 µL of each drug solution was added to each well. One column, though, contained only cells and medium, called a negative control. Another column contained only medium and was used to calculate the background signal from the medium which was deducted from the results. Yet another column was used as a DMSO control. DMSO was diluted in ALT DMEM, so that the DMSO percentage was the same as the dilution of the stock in ALT DMEM to make the highest concentration of drug. Because the drug was dissolved in DMSO, one had to make sure that the DSMO did not have an effect on the cells.

The 96-well plates were incubated for 72 hours. Then 20 µL of 0.1 mg/mL resazurin were added to each of the wells in the 96-well plates. The plates were incubated for four more hours. 0.1 mg/mL resazurin were made by diluting resazurin sodium salt (Sigma-Aldrich, St. Louis, MO, USA) in PBS. After this, a scanning multiwall spectrophotometer (Victor$^3_{TM}$ 1420 multi-label counter, Perkin Elmer, Waltham, MA, USA) was used to “read” the 96-well plates, by measuring the absorbance at dual wavelengths of 560/590 nm. The software WorkOut 2.0 (Dazdag Solution, Perkin Elmer) was used. The data were corrected from the background signal from the medium, and converted into percentage of viable cells in Excel (2013, version: 15.0.4875.1001). A survival rate of 100% was assigned to the control samples, and the samples treated with drug were measured with respect to the control group for each cell line. In Graph Pad Prism v6 software (GraphPad software, Inc, La Jolla, CA, USA) the logarithmic form of the X-values were obtained for further processing of the data

and the Y values were normalized. A normalized response – variable slope logistic nonlinear regression analysis was fitted to the data. The resulting curves demonstrated the cell viability relative to the drug concentration. Three replicates were done for each cell line.

3.3.2 Soft Agar Viability Assay

The soft agar viability assay is an experimental method used to study the cells in 3D. First, a base agar was prepared. 2.4% Difco Agar Noble (Becton, Dickinson and Company, Sparks, USA) were prepared by dissolving 0.48 g powder of Difco Agar Noble (Becton Dickinson Bioscience , NJ, USA) in autoclaved milliQ water. MilliQ water was added until the 20 mL grading on the sterile glass bottle was reached. To dissolve the powder completely, the mixture were microwaved until boiling point and stirred carefully. The solution was transferred to a preheated water bath (50°C) together with 60 mL of ALT DMEM. The 2.4% Difco Agar Noble and ALT DMEM were then mixed in a 1:4 relationship. 50 µL of this solution were pipetted into each well in a 96-well plate by using pre-heated, pre-sterilized disposable pipette tips ART® 100E (molecular BioProducts, Inc., San Diego, CA, USA) and an eight armed pipette. The 96-well plates were left to cool down in room temperature.

The next step was the preparation of the soft agarose overlay. A 2.4% low melting point SIGMA agarose solution was prepared by dissolving 0.48 g SIGMA agarose powder (Sigma-Aldrich, MO, USA) in autoclaved milliQ water. MilliQ water was added until the 20 mL grading on a sterile glass bottle was reached. The mixture was microwaved and stirred until dissolved. Afterwards, the solution was transferred to the preheated water bath (50°C) together with 60 mL ALT DMEM. The 2.4% SIGMA agarose and ALT DMEM were mixed in a 1:4 ratio. The mixture was transferred into sterile conical 15 mL centrifuge tubes (Thermo, Scientific, Nunc, NY, USA) and placed back into the water bath. The temperature was decreased to 40°C.

Cell solutions at 160 000 cells/mL were prepared and kept in 15 mL tubes in the CO_2 incubator. One at a time, the 15 mL tubes with low meting point agarose (mixed with ALT DMEM) was mixed 1:1 with the cell solution. By the use of pre-heated, pre-sterilized disposable pipette tips ART® 100E (molecular BioProducts, Inc., San Diego, CA, USA) and

an eight armed pipette, 50 µL of the mixture was pipette into all of the wells in the 96-well plate on top of the base agar. One exception was the first column, which served as a tool to calculate the background signal. In this column 50 µL of only the SIGMA agarose mixed with ALT DMEM (without any cells) was administered into each well, on top of the base agar. Afterwards, the 96-well plates were refrigerated for 25-30 minutes.

The last step was adding the drug. 100 µL was added to each well and the final concentrations were 0.001 – 0.01 – 0.1 – 0.5 – 1 – 5 – 50 – 100 µM. In addition, a control columns without drug was prepared as well as a column that served as a DMSO-control. Afterwards, the 96-well plates were incubated in the CO_2 incubator at 37°C for 7 days. This assay was done in three replicates for each cell line. After 7 days of incubation, the same procedure as for monolayer (see subchapter 3.3.1) were followed; adding 0.1 mg/mL resazurin, reading the 96-well plates by the use of the scanning multiwall spectrophotometer and analyzing the result by the use of Excel and GraphPad Prism.

3.3.3 Cell Viability - Pictures

Cells were seeded in 6-well plates (Thermo Scientific, Nunc, Roskilde, Denmark) and incubated for 24 hours. Then drug was added to form concentrations of 10, 50 and 100 µM, in addition to negative controls (no drug), and DMSO controls. The cells were incubated for another 72 hours and a Nikon TE2000 light microscope (Nikon Instruments Inc., NY, USA) was used to capture all images, using the 10X objective. For H1_DL2 and H3 100 000 cells per well were used. In contrast, only 50 000 cells per well was used for Melmet 1 pGF1 and Melmet 5 pGF1 owing to their more rapid growth characteristics.

3.4 DNA Cell Cycle Analysis

The cell cycle was analyzed by flow cytometry. Differentiating the cells by size, fluorescence intensity, granularity and count of cells can be done by this procedure (70). These features can in turn be used to analyze cell cycle distribution, which can give us insight into how PJ34 affects the cells.

Cells were cultured in 6-well plates (Thermo Scientific, Nunc, Roskilde, Denmark), with 3 mL of 160 000 cells per well. The plates were incubated for 24 hours in order for the cells to

attach to the surface. 3 mL of PJ34 were added to obtain 50 and 100 µM concentrations. For the negative controls only 3 mL medium were added. DMSO controls were prepared as well. After 24 or 72 hours of incubation the cells were harvested by trypsination, pipetted into 1.5 mL Eppendorf tubes (Eppendorf, Hamburg, Germany) and centrifuged at 1000 rpm for 5 min at 4°C. The Eppendorf tubes were continuously kept on ice. The supernatant was discarded and 1.5 mL ice-cold absolute EtOH (Sigma-Aldrich, MO, USA) was added and resuspended with the pellet. After fixation, the cells could be kept like this in the refrigerator for weeks and even months.

The cells had to be kept in EtOH for a minimum of 24 hours before further analyses could take place. The samples were spun down at 1000 rpm for 5 min at 4°C and the supernatant was discarded. The samples were kept on ice. 50µL 1 mg/mL RNase (Ribonuclease A from bovine pancreas) (Sigma-Aldrich Inc., MO, USA) dissolved in PBS was added to each sample. 150 µL PI (Propidium iodide, 50µg/mL in PBS) (Sigma-Aldrich, MO, USA) was added as well and the cells resuspended. The samples were incubated at room temperature and kept out of light. Then they were transported on ice to the Accuri C6 flow cytometer (Becton Dickinsons Biosciences, NJ, USA). Before running each sample, they were vortexed briefly. To remove doublets gating was done on FL2-A horizontally and FL2-H vertically. The cell counting was stopped after reaching 10 000 cells inside the gate. One also looked at FL2-A versus histogram. The analysis was performed by using FlowJo software (FlowJo, LLC, Ashland, OR, USA). In this software viable cells were gated from debris and other residue, see figure 3.1 A. As mentioned, single cells were gated from the assumed doublets, see figure 3.1 B. In addition, a 2-parameter histogram (FSC-A vs SSC-A), see figure 3.1 C, shows G_1, S and G_2M phases.

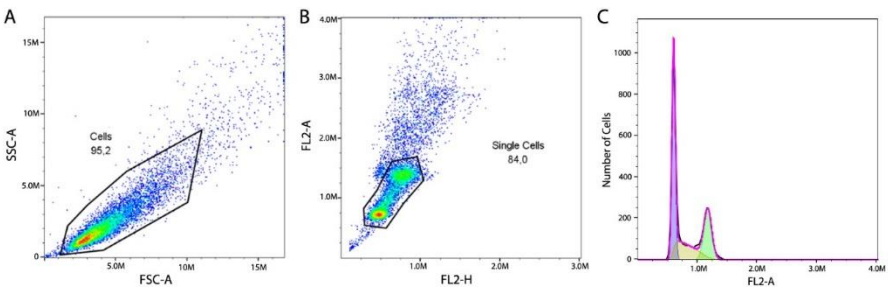

Figure 3.1 – Representation of data analyses in FlowJo: The raw flow cytometry data (A), where single are cells are gated from probable debris (lower left) and doublets (upper right) as shown in the figure. The population is gated to separate the single cells (B) further from the debris, and a histogram showing the cell cycle distribution (C) is also demonstrated. FlowJo has calculated the G_1 phase (purple), S phase (yellow) and G_2M phase (green).

3.5 Apoptosis Assay

100 000 cells were seeded per well in a 6-well plate (Thermo Scientific, Nunc, Roskilde, Denmark). 2 mL of cell solution were used per well. After one day of incubation, drugs were added to the cells giving concentrations of 10, 25- and 50µM of PJ34. Negative controls without drug were also prepared, as well as DMSO controls. After 72 hours the medium was collected from the wells, as this can contain floating apoptotic cells. The wells were washed twice with PBS and this fraction was saved and added to the corresponding previous fraction of medium. The cells were harvested by trypsination using 500 µL 1:1 trypsin (diluted with PBS) per well. After incubation and resuspending of the detached cells with 1 mL medium per well, these fractions were added to previous fractions. The cell fractions were centrifuged at 1000 rpm for 5 minutes to collect a cell pellet. The supernatant was removed and the pellet washed with 1 mL cold PBS before centrifuging the sample again. The supernatant was once again removed and the pellet was resuspended with 50 µL annexin-binding buffer. The annexin binding buffer was prepared in advance using 10 mM HEPES (Sigma-Aldrich, St. Louis, USA), 140 mM NaCl (Sigma-Aldrich, St. Louis, USA) and 2.5 mM $CaCl_2$ (EMD Millipore Corporation, Billerica, MA, USA) at pH 7.4.

The solutions were transferred to 1.5 mL Eppendorf tubes (Eppendorf Ag, Hamburg, Germany). 2.5 µL annexin V Alexa Fluor 647 conjugate (Life Technologies, Eugene, Oregon, USA), 25 µL Propidium iodide (PI) (50 µg/mL) (Sigma-Aldrich Inc., MO, USA) and 20 µL RNase (Sigma-Aldrich Inc., MO, USA) (1 mg/mL in PBS) were added to each sample. After a 15-30 minutes incubation period in room temperature 100-200 µL annexin-binding buffer was added to each sample and mixed gently. All the samples were kept on ice and the samples were analyzed by flow cytometry using Accuri A6 (Becton Dickinsons Biosciences, NJ, USA). The resulting data were analyzed using FlowJo soft weare (FlowJo, LLC, Ashland, OR, USA). Three replicates were performed for each cell line.

3.6 Scratch Wound Healing Assay

One silicone culture insert (Ibidi, Martinsried, Germany) was placed in each well of a 4 well µ-Slide (Ibidi, Martinsried, Germany). 80 µL of 900 000 cells/mL were seeded into each of the two wells in the silicone insert. After the cells had reached 100 % confluency, the inserts were removed which resulted in a gap or a “wound” with a width of approximately 400-450

µm. Each of the wells in the µ-slide was washed with 700 µL ALT DMEM two-three times. Afterwards, 700 µL of drug was added in concentrations of 10, 25 and 50 µM, in addition to a control with only ALT DMEM. By the use of a Nikon TE2000 microscope (Nikon Instruments Inc., NY, USA) pictures of minimum 3 positions on the four wounds were taken every 15 minutes, by the use of the 10X objective. After approximately 72 hours, the images were retrieved. By the use the software Image Pro plus (MediaCybernetics, PA, USA), the images were processed and the wound area in % after specific time points could be calculated, and a graph could be made. The wound size at start (0 hours) was set to 100% and the wound sizes for the treated samples were measured with respect to the wound start size.

3.7 Western Blot

3.7.1 Preparing Lysate

The cells were cultured in medium size (75 cm^2) flasks. Upon reaching approximately 60% confluency, all the medium was removed and 25 mL drug was added. Concentrations used were 10, 25 and 50 µM of PJ34. For the control, only 25 mL medium was added. The flasks were incubated for 48 hours. The cells were harvested by trypsination and transferred to 1.5 mL Eppendorf tubes (Eppendorf, Hamburg, Germany). The samples were centrifuged at 1000 rpm for 4 minutes at 4 °C and the supernatant was discarded. The pellet in the tubes was put on ice and buffer added. If a flask was approximately 60% confluent before trypsination 200 µL buffer was added. The lysis buffer used was RIPA buffer (Sigma-Aldrich, St. Louis, MO, USA) with 1 tablet of phosphatase inhibitor PhosSTOP (Roche Diagnostics, Mannheim, Germany) and 1 tablet of protease inhibitor (Roche Diagnostics, Mannheim, Germany) dissolved per 10 mL RIPA buffer. The buffer was resuspended with the pellet and sonicated with UV sound for 3 x 10 sec (while sample was kept on ice). Afterwards, the samples were centrifuged at 13 000 rpm for 10 min at 4°C. The supernatant was transferred to a new 1.5 mL Eppendorf tube. The supernatant was centrifuged following the same procedure once more. This new supernatant was transferred to yet another 1.5 mL Eppendorf tube and stored in the freezer at -80°C.

3.7.2 Protein Analysis

The samples were thawed on ice. 10 µg/µL BSA in lysis buffer was dissolved and sterile filtered through a 0.2 µm syringe filter (Pall Corporation, Life Sciences, Ann Arbor, MI, USA). 10 µg/µL BSA was used to make several diluted standards (using more lysis buffer)

with the following concentrations: 0.5 - 1.0 - 2.0 - 4.0 - 5.0 µg/µL. BCA working reagent was made from a kit; Pierce™ BCA Protein kit (Thermo Scientific, Rockford, IL, USA), containing reagent A + reagent B. Regent A:B was made in a 50:1 ratio. BCA was prepared with the light off due to its light sensitivity. 200 µL of BCA was pipetted into a 96 well plate in number of standards x 3 wells and number of samples x 3 wells. 2 µL of each of the BSA standards were pipette into the 96-well plate and resuspended with the BCA. In addition, a row of blanks was made containing only BCA and 2 µL lysis buffer. 2 µL of each of the samples was also pipetted onto the 96 well plate and resuspended with the BCA. The plate was wrapped in aluminum foil and incubated for 30 minutes. The plate was afterwards taken to a microplate reader (ASYS UVM 340, Biochrom, Cambridge, UK) using DigiRead and 562 nm measurement. From the results, a linear graph (trend line) was made in Excel by using the standards giving us the equation: y = ax + b. Using the absorbance (y) results from the samples, the protein concentrations of the samples (x), could be determined.

3.7.3 Blotting

Samples of 20 µg were used, and mixed with NuPAGE LDS Sample Buffer 4X (Novex, Carlsbad, CA, USA) and NuPAGE Sample Reducing Agent 10X (Invitrogen, Carlsbad, CA, USA), and milliQ if necessary to reach wanted number of µL of samples. 20 µL in total per sample were used. Afterwards, the samples were incubated for 10 minutes on a heating block. Running buffer was prepared; 50 mL NuPAGE MOPS SDS Running Buffer (novex, Carlsbad, CA, USA) and 950 mL milliQ was mixed together. The gel used was NuPAGE 4-12 % Bis-Tris gel, 1.5 mm, 10 well or 12 well (Novex, Carlsbad, CA, USA). The comb of the gel cassette was removed and the wells rinsed using running buffer. The cassette was placed in a container, called “the Mini-Cell” (Invitrogen Novex, Carlsbad, USA), and a gel tension wedge (Invitrogen Novex, Carlsbad, USA) was used to hold the cassette in place. The Mini-Cell was in turn placed in a box of ice. 200 mL of the running buffer were added 500 µL NuPAGE ® Antioxidant (metylformarmide) (Invitrogen, Carlsbad, USA). These 200 mL were used to fill the upper (inner) buffer chamber to just over the edge of the gel. The lower (outer) buffer chamber was filled with running buffer as well.

10 µl of the standard SeeBlu®Plus2 Prestained Standard (1X) (Invitrogen, Carlsbad, USA) was pipetted into one well. Continuing from right to left with 20 µL of sample 1 (= control), 2 (= 10 µL drug), 3 (= 25µL drug) and 4 (= 50 µL drug). To pipette the standard and samples a

special kind of pipette tips were used, called Prot/Elec^{TM} Tips (BioRad, USA). The lid (Invitrogen novex, Carlsbad, USA) of the western blotting container was place on top, and the wires connected. 200 V was applied for 55 minutes.

In the meantime, transfer buffer was prepared. 50 mL NuPAGE MOPS transfer buffer (20X) (Novex, Carlsbad, USA) was mixed together with 1 mL antioxidant (same one as described above), 849 mL MilliQ water and 100 mL methanol. Approximately 4 to 7 pads were soaked in transfer buffer and air bubbles removed by squeezing the pads while in buffer. Nitrocellulose blotting membrane 0.2 µm (GE Healthcare, Life Sciences, Germany) and 2 pieces of filter paper were cut out in the same size as the pads. Afterwards the assembly of the gel membrane sandwich began. Two pads were place in the cathode (-) core, which constituted the bottom of the blot module (Invitrogen novex, Carlsbad, USA). After the run from earlier was completed the gel cassette was removed from the Mini-Cell and the cassette opened. Then the filter paper was placed on the gel and the filter paper was faced downwards in the sandwich. The gel top was covered with the membrane piece, which was topped with a piece of filter paper and needed number of pads. One had to have enough pads to create a resistance inside the box. The anode (+) core was used as a lid on the gel sandwich assembly. The blot module had to be held together firmly and slid into the guide rails of the lower buffer chamber (Invitrogen novex, Carlsbad, USA). A gel tension wedge was used to hold the blot module in place. This container was also placed on ice. The blot module was filled with transfer buffer in the upper chamber, and cold tap water was used to fill the lower buffer chamber. The lid (Invitrogen novex, Carlsbad, USA) was placed on top of the unit and the wires connected. 30 V was applied for 90 minutes.

Meanwhile, a wash solution, TBST, was prepared. TBS 10X (Sigma-Aldrich Inc., St. Louis, MO, USA) was diluted with milliQ. To make TBST, 0.1 % Tween 20 (Sigma-Aldrich Inc., St. Louis, MO, USA) was added to the 1X TBS. Blocking buffer was also prepared. This contained a mix of fat free dry milk (Difco Skim Milk BD, Sparks, MD, USA) and TBST. For 50 mL in total, 2.5 g dry milk was used. After the 90 minutes of applied voltage on the gel was complete, the nitrocellulose membrane was removed from the container, and rinsed with Ponceau solution (Sigma-Aldrich Inc., St. Louis, MO, USA) until bands appeared on the membrane. Transparent paper was laid under and above the membrane and was cut into as

many pieces as antibodies used for this membrane. The pieces were placed in separate containers in a plastic box with a lid. 3 mL blocking solution were added to each membrane piece (fully covering the membrane) and the membranes were incubated for one hour in room temperature under agitation, using a see-saw rocker with 18-23 osc/min. By blocking the membrane, one prevents non-specific background binding of the primary and/or secondary antibodies to the membrane (76). Afterwards the blocking solution was replaced with 3 mL of fresh blocking solution containing primary antibody for each membrane piece.

Primary antibodies used in this thesis were: Anti-PARP, anti-phospho-Akt(S473), anti-phospho-Akt(T308), anti-Rad51 and anti-GAPDH (as a loading control) all from rabbits and Cell Signaling Technology Boston, Ma, USA. For anti – GAPDH and anti – Rad51 a dilution of 1:5000 and 1:2000 was used respectively. For the remaining primary antibodies a dilution of 1:1000 was used. To hinder evaporation Para-film was wrapped around the box containing the membranes. The box was incubated over night at 4 °C under agitation (using a see-saw rocker at approximately 11 osc/min.) It is important to incubate at 4 °C to hinder contamination and thus destruction of the protein. Agitation is preferably used to prevent uneven binding and ensure adequate homogenous covering of the membrane (76).

On the next day, the membrane pieces were washed quickly approximately five times, with the wash solution, TBST. Afterwards, washing with TBST was done 2-3 times, for 5-10 min under rapid agitation. This was done to remove all remaining primary antibody. Secondary antibody used, was dissolved in blocking solution. Anti-Rabbit (HRP-conjugated) (Beckman coulter, Marseille, France) was used as secondary antibody for all the primary antibodies. Anti-Rabbit was diluted to 1:20 000 in blocking solution. 3 mL of secondary antibody in blocking solution was used per membrane. Incubation followed for two hours in room temperature under agitation (using a see-saw rocker). After incubation the membranes were washed quickly approximately five times with TBST, and two times for 5-10 minutes under rapid agitation. ECL (chemiluminisensce) kit; West PICO or WEST FEMT (Both from Thermo Scientific, Rockford, Il, USA) was used on the membranes. A 1:1 solution of ECL was prepared and shielded as much as possible from light, due to its light sensitivity. The membrane pieces were soaked in milliQ water and brought to the reading machine (Fujifilm LAS3000, Intelligent DarkBox). Before each membrane was read, it was transported onto a

transparent piece, soaked in ECL and incubated for 1 minute. Then a transparent piece was placed on top and the reading could begin. The machine was pre-cooled to – 25°C and pictures was taken using different exposure times.

3.8 Spheroid Measurements

Multicellular spheroids were prepared in order to study the drug effect on 3D tumors. Spheroids more accurately mimics *in vivo* tumor tissue than 2D cell monolayers (77).
The cells were cultured in a Costar 96-well round bottom ultra-low attachment plate (Corning Inc., Corning, NY, USA), using 4 000 cells per well. The plate was centrifuged at 1 000 g for 15 minutes and stored in the incubator (at 37°C) for 6 days, after which the tumor spheroids had formed. Then drug was added to the 96-well plate giving concentrations of 10, 15- and 50 µM PJ34. DMSO controls and negative controls were also prepared. This was named day 0. A Nikon TE2000 light microscope (Nikon Instruments Inc., NY, USA) was used to capture images of the spheroids using a 4X objective. Images of eight spheroids were captured per drug concentration. To measure the spheroids, Fiji Image J software (win. 64, Maryland, USA) was utilized. By measuring the longest and the shortest diameter of each spheroid in µm, a mean diameter could be found. This mean diameter was used to compare the spheroids sizes. Images were captured of the spheroids using Nikon every 4 day for 20 days.

3.9 In Vivo

All animal procedures were approved by the National Animal Research Authority. The animals were kept in an animal facility under standardized conditions. They were fed a diet of standard pellets and were provided water *ad libitum.*

3.9.1 Cell Preparations

The H1_DL2 cell line was injected into the mice. 5 000 000 cells/mL was prepared in PBS. A 100 µL of this solution (i.e. 500 000 cells) were injected subcutaneously in to the neck area of each mouse. The neck was shaved, to give a better view of the needle while injecting. Needles used for the injections were 0.5 mL single-use insulin syringes with integrated needles (Omnican B. Braun, Melsungen, Germany).

3.9.2 Drug Injections

Ten immunodeficient female NOD/SCID mice were used in this experiment. 10 mg/ kg of PJ34 (diluted in PBS) was injected intraperitoneally to five mice whereas only PBS was

injected in the other five mice. Again, the needle types used were 0.5 mL single-use insulin syringes with integrated needle (Omnican B. Braun, Melsungen, Germany). A 20 gram mice was given 100 µL injection of PJ34 diluted 2:1 in PBS. The intraperitoneal injections were performed three times a week for three weeks. After this, the injection-dose was increased to 300 µL for a 20 gram mouse using the same drug dilutions as before. This means that the drug dosage was increased to 30 mg/kg of PJ34. In addition to the injections, the mice were also weighed, and their tumors measured, three times a week. The tumor of each mouse was measured by using an electronic caliper. The longest and the shortest diameter of each tumor was measured, giving us a length and a width. The volume of the tumors were calculated by the use of the following equation: Volume = 0.5 x length x width^2 (78).

3.9.3 Western Blotting - Tumors

Western blotting from six tumors was also performed, using the tumors from three control mice (B50M1, B50M2 and B50M4) and three drug treated mice (B51M1, B51M2 and B51M3). The tumors that would be used for western blotting were frozen in nitrogen immediately after removal from the animals. The remaining tumor were kept refrigerated in 4 % formaldehyde diluted with PBS from a 16% formaldehyde solution (Thermo Scientific, Rockford, IL, USA) for possible future work.

After being frozen in nitrogen for about 24 hours, the tumors were cut into 10 µm slices using the Cryostat LEICA CM 3050S (Leica Biosystems, Wetzlar, Germany) The temperature in the cryostat were set to -20°C and the samples were kept on dry ice at all times (except when slicing). The tumor slices were collected in 2.5 mL Eppendorf tubes (Eppendorf AG, Hamburg, Germany) and frozen at -80°C for about 24 hours. Afterwards, the samples were kept continuously on ice, and RIPA buffer with phosphatase inhibitor and protease inhibitor were added to the different tubes. Further homogenization was achieved by using a small electronic blending stick for 3 x 5 seconds on each sample. Afterwards the samples were sonicated with UV sound for 3 x 10 sec (again while sample was kept on ice). This was done twice. Then the samples were centrifuged at 13 000 rpm for 10 min at 4°C. The supernatant was transferred to a new 1.5 mL Eppendorf tube. The supernatant was centrifuged by following the same procedure once more. This new supernatant was transferred to yet another 1.5 mL Eppendorf tube and stored the freezer at -80°C. After this was completed, protein analysis and western blotting could be performed in the same way as described in subchapters 3.7.2 and 3.7.3.

4 Results

4.1 Cell Viability Assays

4.1.1 Monolayer Viability Assay

The monolayer proliferation assay was used to study viability of the metastatic cell lines after treatment with increasing concentrations of PJ34.

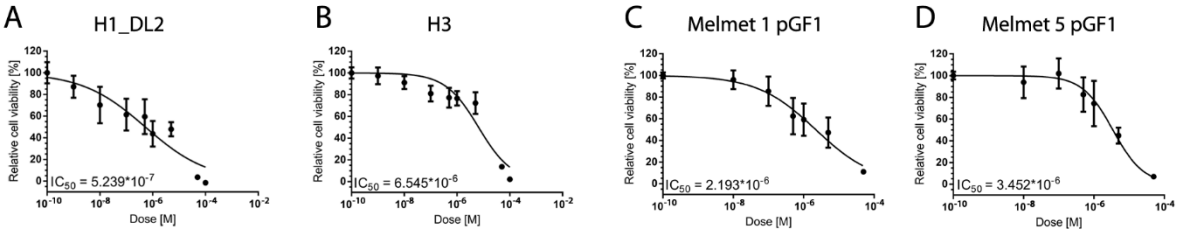

Figure 4.1 – Monolayer viability assay, tumor cells: The cells were treated for 72 h with increasing concentrations of PJ34 to investigate the possible inhibitory effect of the drug on the cells. The experiment was repeated three times for each cell line, thus the four graphs shown here are the ones that have an IC_{50} dose closest to the mean IC_{50} dose.

Figure 4.1 show the most representative results of the monolayer proliferation assay. The relative viability in percentage (Y – axis) were plotted against the logarithmic dosage of PJ34 in molar (X – axis). The graphs in figure 4.1 shows a sigmoidal shape, especially in figure 4.1 B and D. For all four cell lines, an increase in drug doses resulted in reduction in cell viability. At concentrations of 50- and 100 µM less than 20% of the cells were viable. IC_{50} doses varied between 0.5 and 6.5 µM.

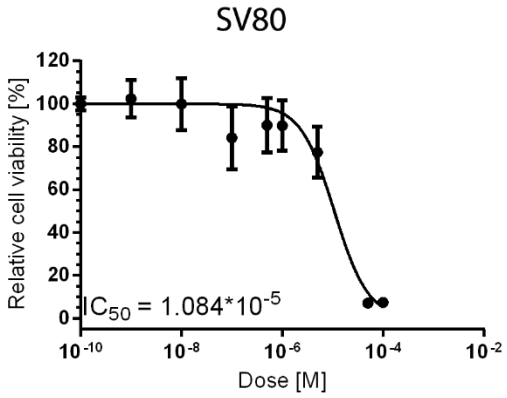

Figure 4.2 – Monolayer viability assay, SV80: The cells were treated for 72 h with increasing concentrations of PJ34 to investigate any possible inhibitory effect of the drug on the SV80 cells. The experiment was repeated three times, thus the graph shown here are the one that has an IC_{50} dose closest to the mean IC_{50} dose.

For the normal endothelial cell line SV80, an increase in drug dosage resulted in decreased cell viability, but the cells were less responsive than the tumor cell lines.

Table 4.1- Monolayer Viability Assay: Shows the mean IC_{50} dosage ± the standard deviation ($*10^{-6}$) for all four tumor cell lines; H1_DL2, H3, Melmet 1 pGF1 and Melmet 5 pGF1 including the fibroblast cell line SV80.

Monolayer proliferation assay	
Cell-line	*Mean IC_{50} ± SD [$*10^{-6}$ M]*
H1_DL2	1.084 ± 1.005
H3	6.213 ± 4.153
Melmet 1 pGF1	2.723 ± 2.578
Melmet 5 pGF1	3.178 ± 0.772
SV 80	10.552 ± 2.097

Table 4.1 shows the mean IC_{50} dosages for all cell lines used. The IC_{50} dose is the drug concentration were 50 % of the cell are viable. The mean IC_{50} dosage for SV80 was in the 10^{-5} range, while the tumor cell lines had a mean IC_{50} in the 10^{-6} range. H3 was the tumor cell line with the highest mean IC_{50} dose.

4.1.2 Soft Agar Viability Assay

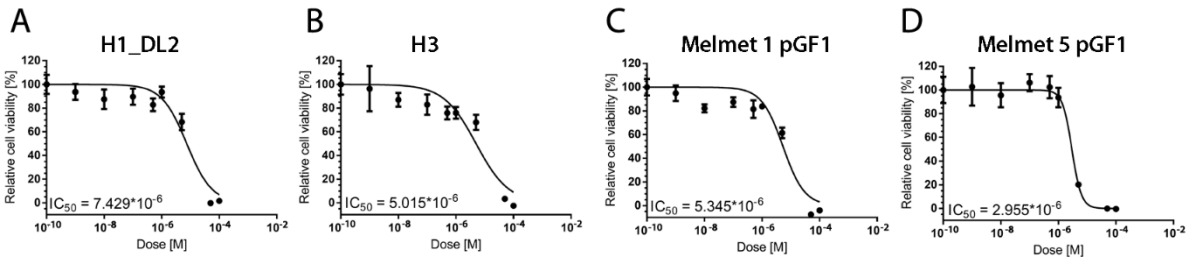

Figure 4.3 – Soft agar viability assay: The cells were treated for 72 h with different concentrations of PJ34 to investigate any possible inhibitory effect of the drug on the cells. The experiment was repeated three times for each cell line, thus the four graphs shown here are the ones that have an IC_{50} dose closest to the mean IC_{50} dose.

Figure 4.3 shows the most representative results for the soft agar viability assay.
The relative viability in percentage (Y – axis) was plotted against the logarithmic dosage of PJ34 in molar (X – axis). The graphs in figure 4.3 shows a sigmoidal shape and a correlation between increased drug dosage and decreased cell viability.

Table 4.2 – Soft agar viability assay: Shows the mean IC_{50} dosage ± the standard deviation ($*10^{-6}$) for all four tumor cell lines; H1_DL2, H3, Melmet 1 pGF1 and Melmet 5 pGF1.

Soft agar viability assay	
Cell-line	*Mean IC_{50} ± SD ($*10^{-6}$ M)*
H1_DL2	7.527 ± 0,371
H3	4.537 ± 1.813
Melmet 1 pGF1	5.026 ± 1.251
Melmet 5 pGF1	2.821 ± 0.328

In table 4.2 the mean IC_{50} dosages of all the metastatic melanoma cell lines are shown. Here H1_DL2 was the tumor cell line with the highest mean IC_{50} dose. The SV80 cell line was not tested.

Comparing the IC_{50} doses for monolayer proliferation assay (see table 4.1) and soft agar colony forming assay (see table 4.2), we observed that the results were mainly quite similar.

4.1.3 Cell Viability - Pictures

Using the Nikon TE2000 inverted microscope, images of treated and untreated cells for all four tumor cell lines, including the fibroblast cell line SV80, was obtained. All the images were capture while using a 10X objective.

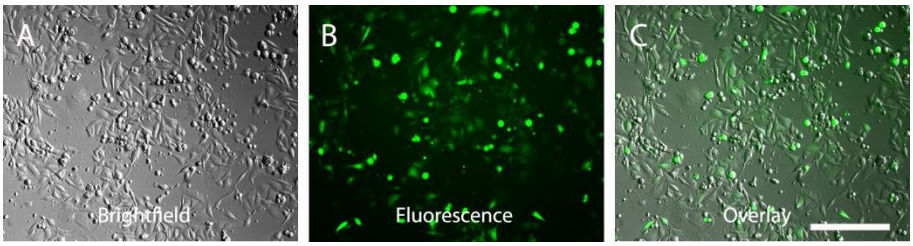

Figure 4.4 – Cell viability - pictures: Images of untreated H1_DL2 cells (controls) using brightfield (A), fluorescence microscopy (B) and overlay of both previous images (C). Scale bar = 500 µm.

Figure 4.4 shows that the green fluorescent protein is functioning well in staining the H1_DL2 cells. Similar pictures were taken for all cell lines with fluorescence, and confirmed that the green fluorescence protein functioned as expected (data not shown).

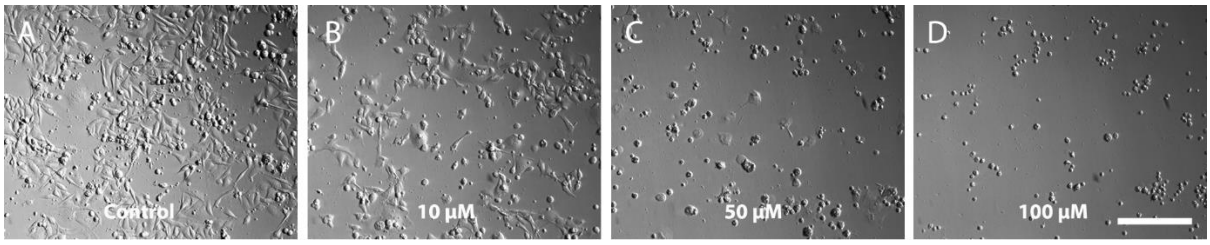

Figure 4.5 – Cell viability - pictures: Images demonstrating cell morphology and the effect of drug (PJ34) on H1_DL2 cells. The figure shows a control of untreated cells (A) and cells treated with 10 µM (B), 50µM (C) and 100 µM (D) of PJ34. Scale bar = 500 µm.

Figure 4.5 A shows that most of the untreated H1_DL2 cells had an elongated shape, while some were more round, maybe due to mitosis, and the cells grew mainly in patches. While adding drug and increasing the dosage through figures 4.5 B, C and D, the images shows that the H1_DL2 cells first became rounder and afterwards smaller, and cell numbers decreased.

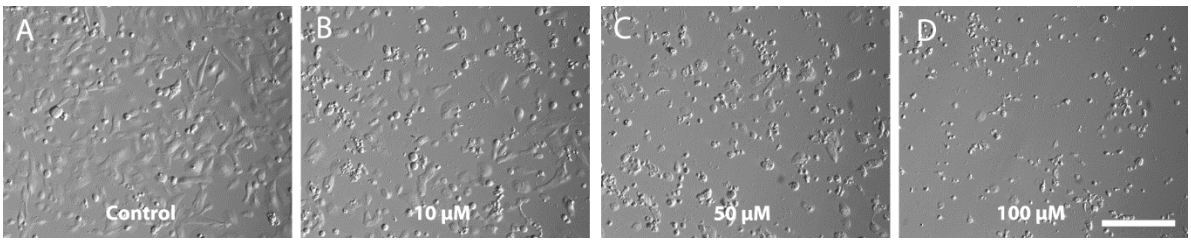

Figure 4.6 – Cell viability - pictures: Images demonstrating cell morphology and the effect of drug (PJ34) on H3 cells. The figure shows a control of untreated cells (A) and cells treated with 10 µM (B), 50µM (C) and 100 µM (D) of PJ34. Scale bar = 500 µm.

Figure 4.6 A show that the untreated H3 cells grew quite evenly distributed. Also here most of the cells were large and elongated, while a few cells were small and round. While increasing the drug dosage through figures 4.6 B, C and D, the images shows that the H3 cells decreased in size, rounded up and also decreased greatly in number.

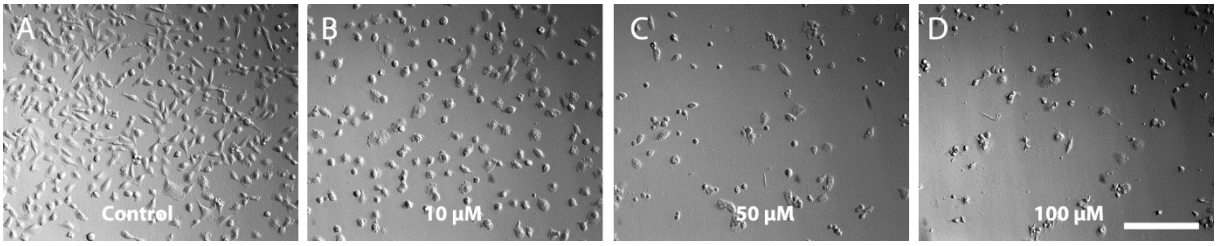

Figure 4.7 – Cell viability - pictures: Images demonstrating cell morphology and the effect of drug (PJ34) on Melmet 1 pGF1. The figure shows a control of untreated cells (A) and cells treated with 10 µM (B), 50µM (C) and 100 µM (D) of PJ34. Scale bar = 500 µm.

Figure 4.7 A shows that the untreated Melmet 1 pGF1 cells grew evenly distributed and also were somewhat elongated. As the concentration of PJ34 increased (figures 4.7 B-D), the

Melmet 1 pGF1 cells first rounded up and increased some in size and then became smaller and decreased in number.

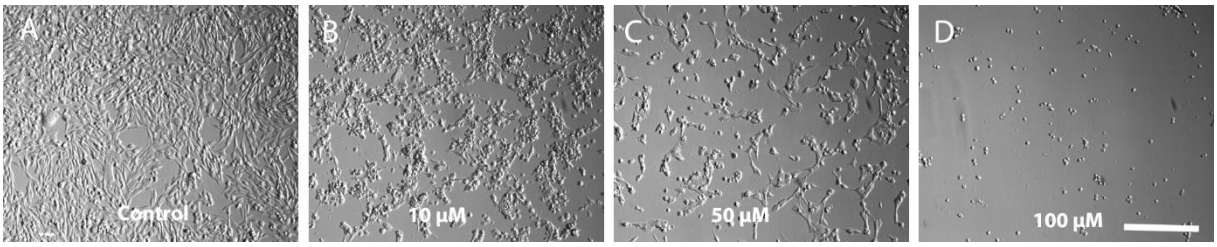

Figure 4.8 – Cell viability - pictures: Images demonstrating cell morphology and the effect of drug (PJ34) on Melmet 5 pGF1 cells. The figure shows a control of untreated cells (A) and cells treated with 10 µM (B), 50µM (C) and 100 µM (D) of PJ34. Scale bar = 500 µm.

Figure 4.8 A shows that the untreated Melmet 5 pGF1 cells grew in large patches and had an elongated shape. At a drug concentration of 10 µM (figure 4.8 B) the Melmet 5 pGF1 became more round, and divided even more into patches. A great decrease in cell number could be seen throughout figure 4.8 B-D. Here as well, there was a correlation between increased concentration of PJ34 and reduced cell numbers.

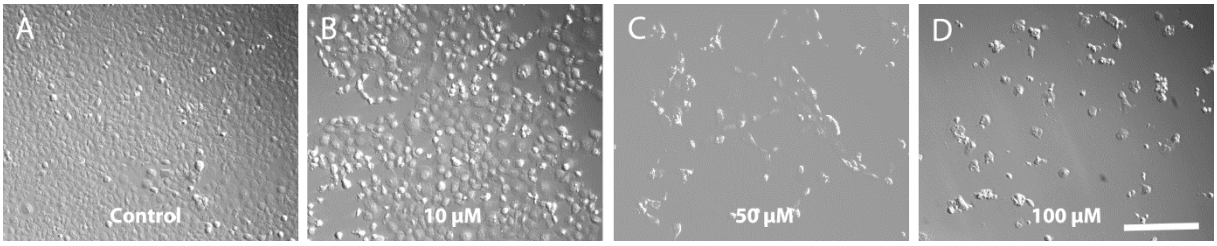

Figure 4.9 – Cell viability - pictures: Images demonstrating cell morphology and the effect of drug (PJ34) on SV80 cells. The figure shows a control of untreated cells (A) and cells treated with 10 µM (B), 50µM (C) and 100 µM (D) of PJ34. Scale bar = 500 µm.

Figure 4.9 A shows an image of untreated SV 80 cells, and they appear to be quite round. With increasing drug dose (figures 4.9 B-D) the cells became somewhat larger and fewer in number as well as clumping together.

In general, it was observed for all cell lines that there were a correlation between increased drug dose and reduced number of cells.

4.2 DNA Cell Cycle Analyses

Flow cytometry was used study the distribution of the cells in the cell cycle before and after treatment of the tumor cells. Before comparing the results, notice that the Y-axis are not in the same scale in the different histograms in the figures beneath.

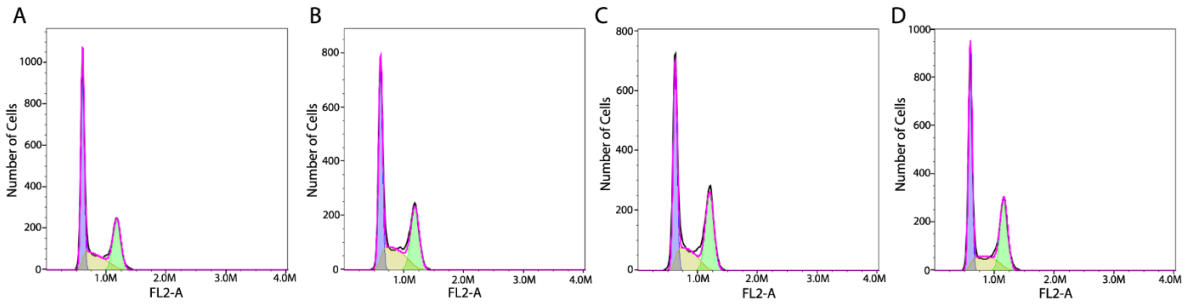

Figure 4.10 – Cell cycle analysis of H1_DL2 using flow cytometry: For each experiment, one well served as a control (A) and the others had been added 10 µM (B), 25 µM (C) and 50 µM (D) drug. Three replicates were done for each cell line, thus the four graphs shown here are the ones that were the most representative for this cell line.

The distribution of H1_DL2 cells in different phases of the cell cycle before and after treatment is shown in Figure 4.10. Treatment with either 10 µM (Figure 4.10 B), 25 µM (Figure 4.10 C) or 50 µM (Figure 4.10 D) for 24 hours did not appear to alter the distribution of cells in the different phases of the cell cycle.

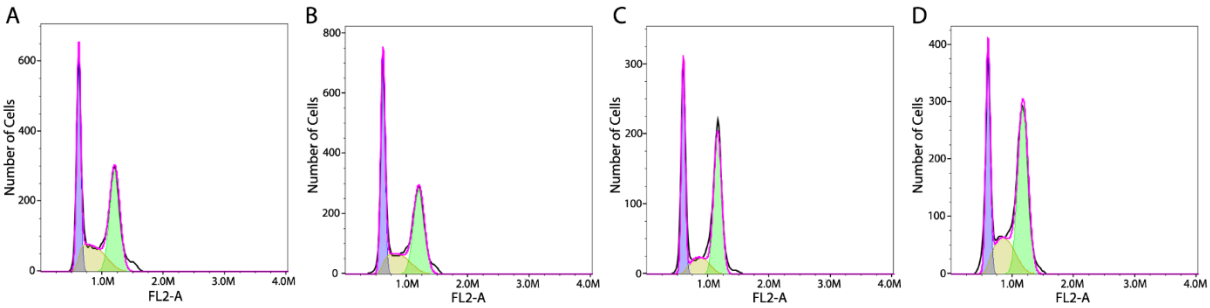

Figure 4.11 – Cell cycle analysis of H3 using flow cytometry: For each experiment, one well served as a control (A) and the others had been added 10 µM (B), 25 µM (C) and 50 µM (D) drug. The experiment was repeated three times for each cell line, thus the four graphs shown here are the ones that were the most representative for this cell line.

The distribution of H3 cells in different phases of the cell cycle before and after treatment is shown in Figure 4.11 (24 hours of treatment). A decrease in G_1 – and S phase and an increase in G_2M phase is shown after treatment with 25- and 50 µM PJ34.

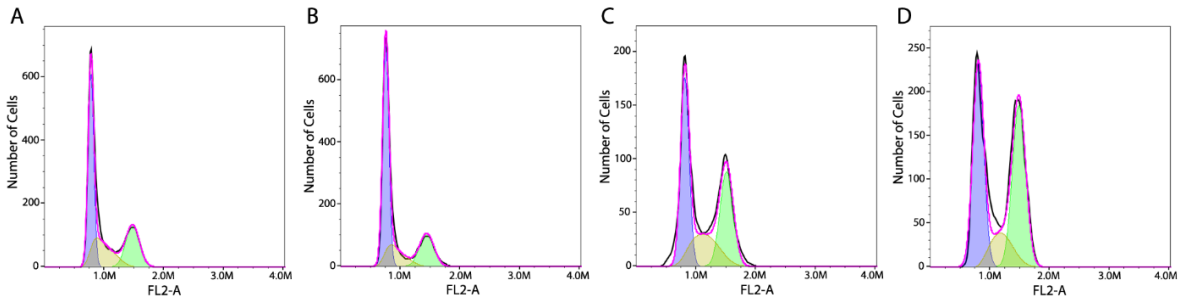

Figure 4.12 – Cell cycle analysis of Melmet 1 pGF1 using flow cytometry: For each experiment, one well served as a control (A) and the others had been added 10 µM (B), 25 µM (C) and 50 µM (D) drug. Three replicates were performed for each cell line, thus the four graphs shown here are the ones that were the most representative for this cell line.

Figure 4.12 shows the distribution of Melmet 1 pGF1 cells in different phases of the cell cycle before and after 24 hours of treatment. A decrease in G_1 phase is shown after treatment with both 25- and 50 µM PJ34. However, only after treatment with 50 µM an increase in G_2M phase is clearly seen.

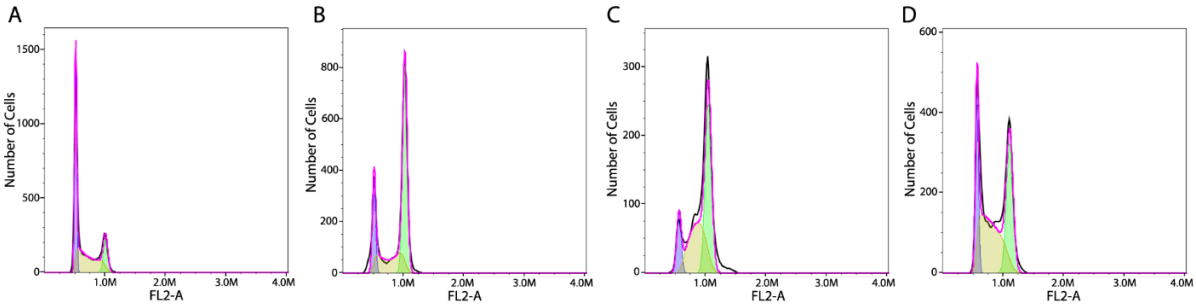

Figure 4.13 – Cell cycle analysis of Melmet 5 pGF1 using flow cytometry: For each experiment, one well served as a control (A) and the others had been added 10 µM (B), 25 µM (C) and 50 µM (D) drug. Three replicates were done for each cell line, thus the four graphs shown here are the ones that were the most representative for this cell line.

Figure 4.13 shows the distribution of Melmet 5 pGF1 cells in different phases of the cell cycle before and after 24 hours of treatment. A decrease in G_1 phase and an increase in G_2M phase is shown after treatment with all the tree different concentrations of PJ34

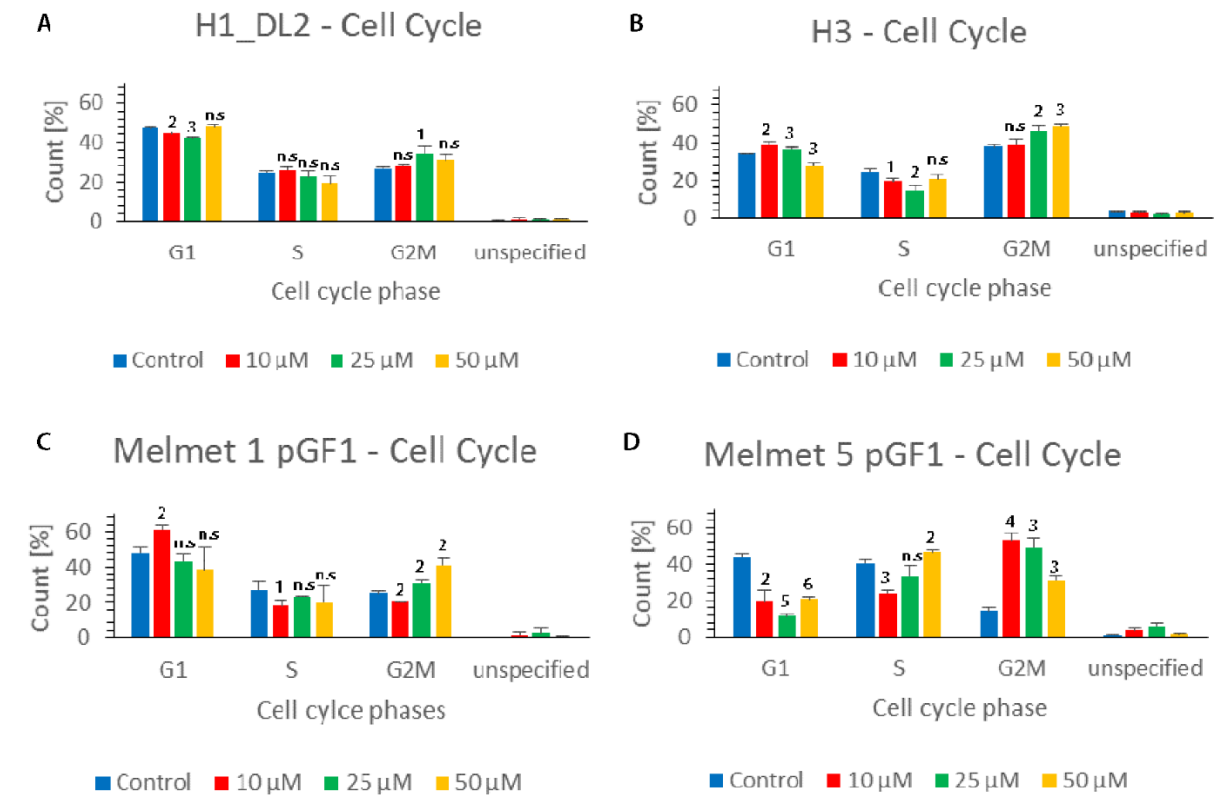

Figure 4.14 – Change in cell cycle distribution: For each of the four tumor cell lines; H1_DL2 (A), H3 (B). Melmet 1 pGF1 (C) and Melmet 5 pGF1 (D), the count of cells in the different stages of the cell cycle are compared between controls and cells treated with 10, 25 and 50 µM PJ34 for 24 hours. Three replicates were performed for each cell line, thus the graphs shows the mean value + the standard deviation of the distributions of the cells in G_1, S and G_2M phases. Double sided t-test was performed for each concentration compared to the control in G_1, S and G_2M phase. n.s = not significant, 1 = $p \leq 0.05$, 2 = $p \leq 0.01$, 3 = $p \leq 0.001$, 4 = $p \leq 0.0001$, 5 = $p \leq 0.00001$, 6 = $p \leq 0.000001$.

Figure 4.14 shows that especially Melmet 1 pGF1 and Melmet 5 pGF1 demonstrate a shift from G_1 to G_2M phase, while H1_DL2 and H3 does not have that clear results.

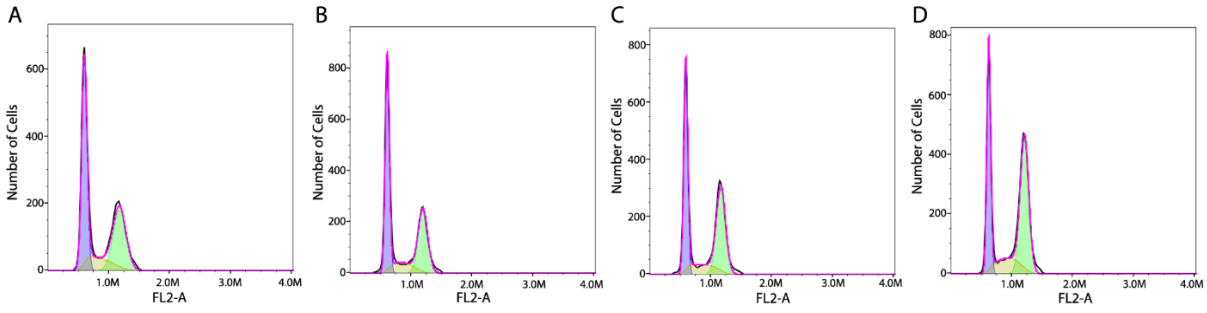

Figure 4.15 – Cell cycle analysis of H3 using flow cytometry (72 h): For each experiment, one well served as a control (A) and the others had been added 10 µM (B), 25 µM (C) and 50 µM (D) drug. Three replicates were done for each cell line, thus the four graphs shown here are the ones that were the most representative for this cell line.

The distribution of H3 cells in different phases of the cell cycle before and after treatment with PJ34 for 72 hours is shown in figure 4.15. An increase in G_2M phase is shown after treatment with 25 and 50 µM PJ34.

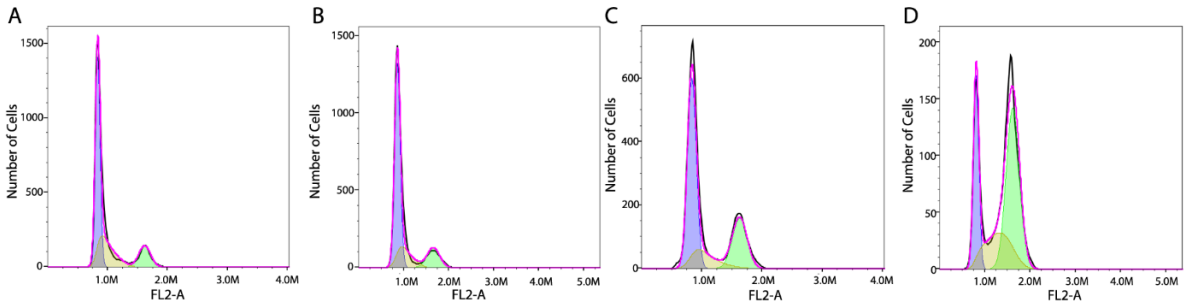

Figure 4.16 – Cell cycle analysis of Melmet 1 pGF1 using flow cytometry (72 h): For each experiment, one well served as a control (A) and the others had been added 10 µM (B), 25 µM (C) and 50 µM (D) drug. The experiment was repeated three times for each cell line, thus the three graphs shown here are the ones that were the most representative for this cell line.

Figure 4.16 shows the distribution of Melmet 1 pGF1 cells in different phases of the cell cycle before and after treatment with PJ34 for 72 hours. A decrease in G_1 phase and an increase in G_2M phase is shown after treatment with 25- and 50 µM drug.

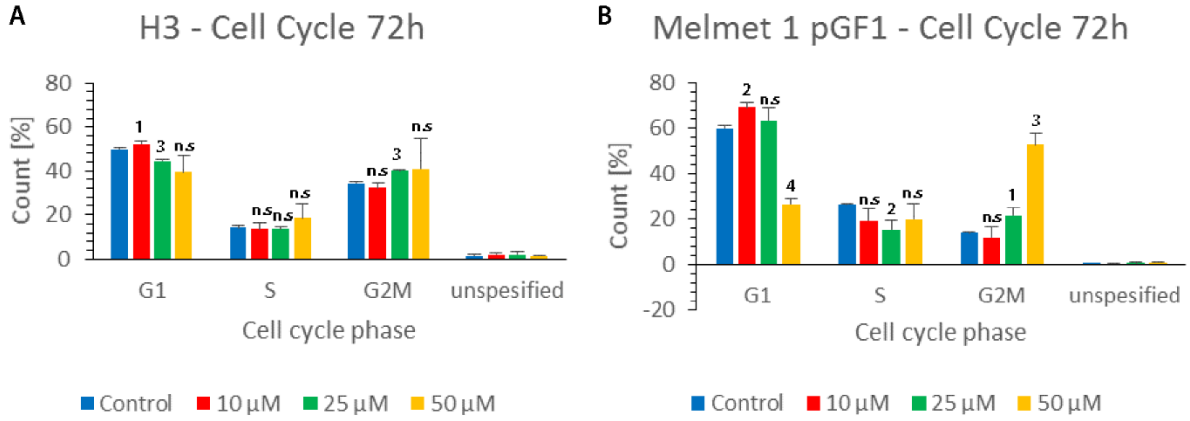

Figure 4.17 – Change in cell cycle distribution (72 h): For two of the four tumor cell lines; H3(A), Melmet 1 pGF1 (B), the count of cells in the different stages of the cell cycle are compared between controls and cells treated with 10, 25 and 50 µM PJ34 for 72 hours. Three replicates were performed for each cell line, thus the graphs shows the mean value + the standard deviation of the distributions of the cells in G_1, S and G_2M phases. Double sided t-test was performed for each concentration compared to the control in G_1, S and G_2M phase. n.s = not significant, 1 = $p \leq 0.05$, 2 = $p \leq 0.01$, 3 = $p \leq 0.001$, 4 = $p \leq 0.0001$, 5 = $p \leq 0.00001$, 6 = $p \leq 0.000001$.

Figure 4.17 shows that for H3 only treatment with 25 µM has a statistically significant decrease in G_1 phase as well as a significant increase in G_2M phase compared to the control. For Melmet 1 pGF1 only treatment with 50 µM drug has a statistically significant decrease in G_1 phase and significant increase in G_2M phase compared to the control. After treatment for 72 hours with different drug dosages, the result does generally not seem to offer an increased shift from G_1 to G_2M phase compared to after treatment for 24 hours (see figure. 4.14). Due to these results as well as the time constraint, the H1_DL2 and the Melmet 5 pGF1 cell lines were not tested for 72 hours of treatment.

4.3 Apoptosis Assay

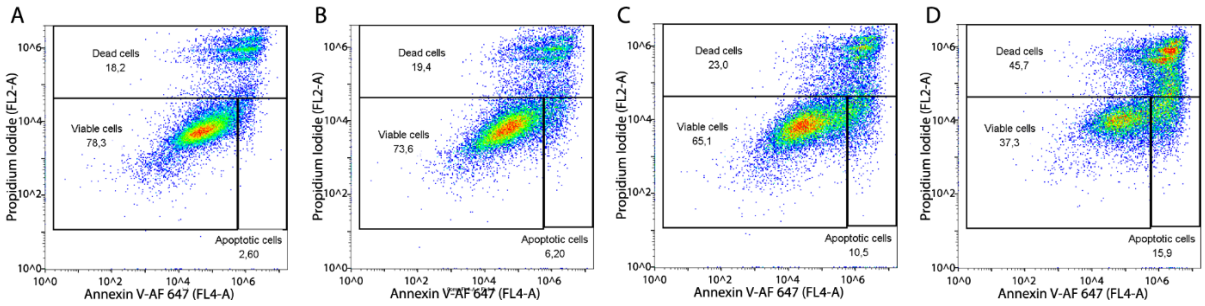

Figure 4.18 – Apoptosis assay of H1 using flow cytometry: For each experiment, one well served as a control (A) and the others had been added 10 µM (B), 25 µM (C) and 50 µM (D) drug. Three replicates were done, thus the four graphs shown here are the ones that were the most representative for this cell line.

The distribution of H1 cells in different states (viable, apoptotic or dead) for control and treatment is shown in Figure 4.18. Number of viable cells decreased with increasing drug dosage and the number of apoptotic and dead cells increased.

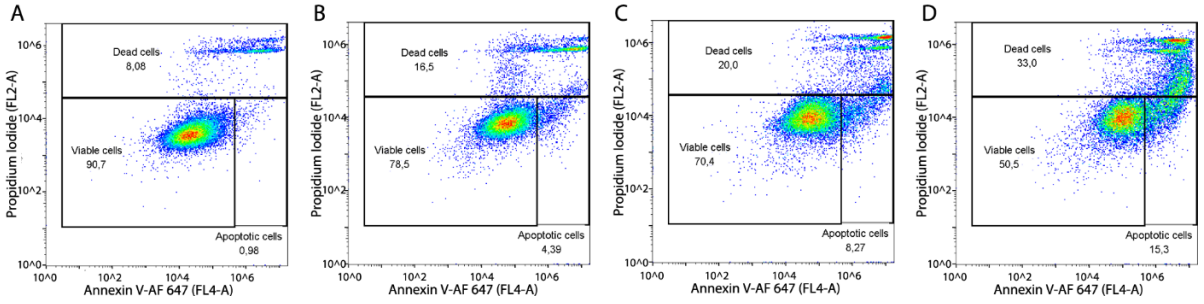

Figure 4.19 – Apoptosis assay of H3 using flow cytometry: For each experiment, one well served as a control (A) and the others had been added 10 µM (B), 25 µM (C) and 50 µM (D) drug. The experiment was repeated three times, thus the four graphs shown here are the ones that were the most representative for this cell line.

Figure 4.19 shows the distribution of the H3 cells in viable, apoptotic or dead states for control and treated samples. Here too, the number of viable cells decreased and the number of apoptotic and dead cells increased, with increasing drug dosage.

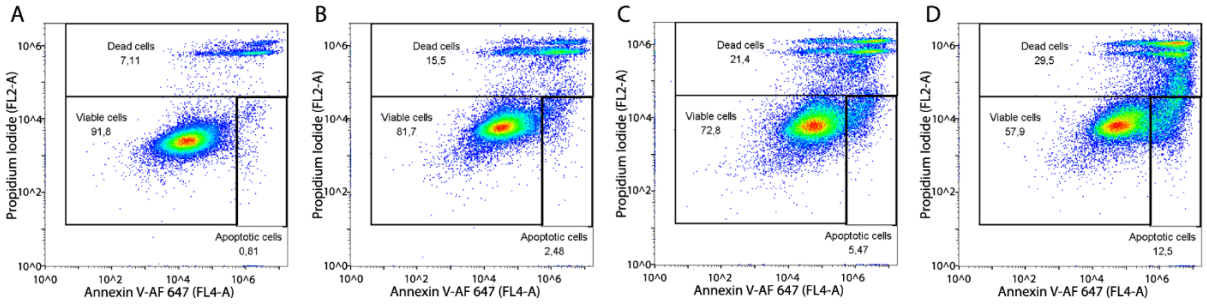

Figure 4.20 – Apoptosis of Melmet 1 using flow cytometry: For each experiment, one well served as a control (A) and the others had been added 10 µM (B), 25 µM (C) and 50 µM (D) drug. Three replicates were done, thus the four graphs shown here are the ones that were the most representative for this cell line.

Figure 4.20 shows the percentage of Melmet 1 cells in viable, apoptotic or dead states for control and treated samples. As the drug dosage became higher, the fewer cells became viable and more cells become apoptotic or dead.

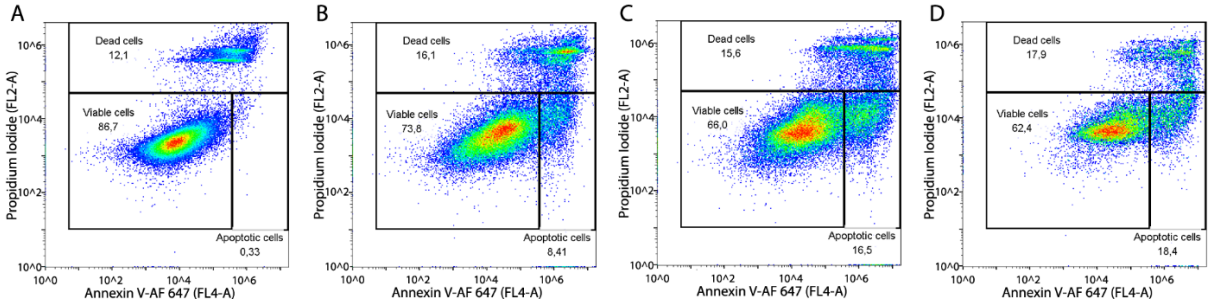

Figure 4.21 – Apoptosis of Melmet 5 using flow cytometry: For each experiment, one well served as a control (A) and the others had been added 10 µM drug (B) , 25 µM drug (C) and 50 µM drug (D). Three replicates were performed, thus the four graphs shown here are the ones that were the most representative for this cell line.

The distribution of Melmet 5 cells in different states (viable, apoptotic or dead) for control and treated samples are shown in Figure 4.21. Number of viable cells decreased and the number of apoptotic cells increased with increasing drug dosage.

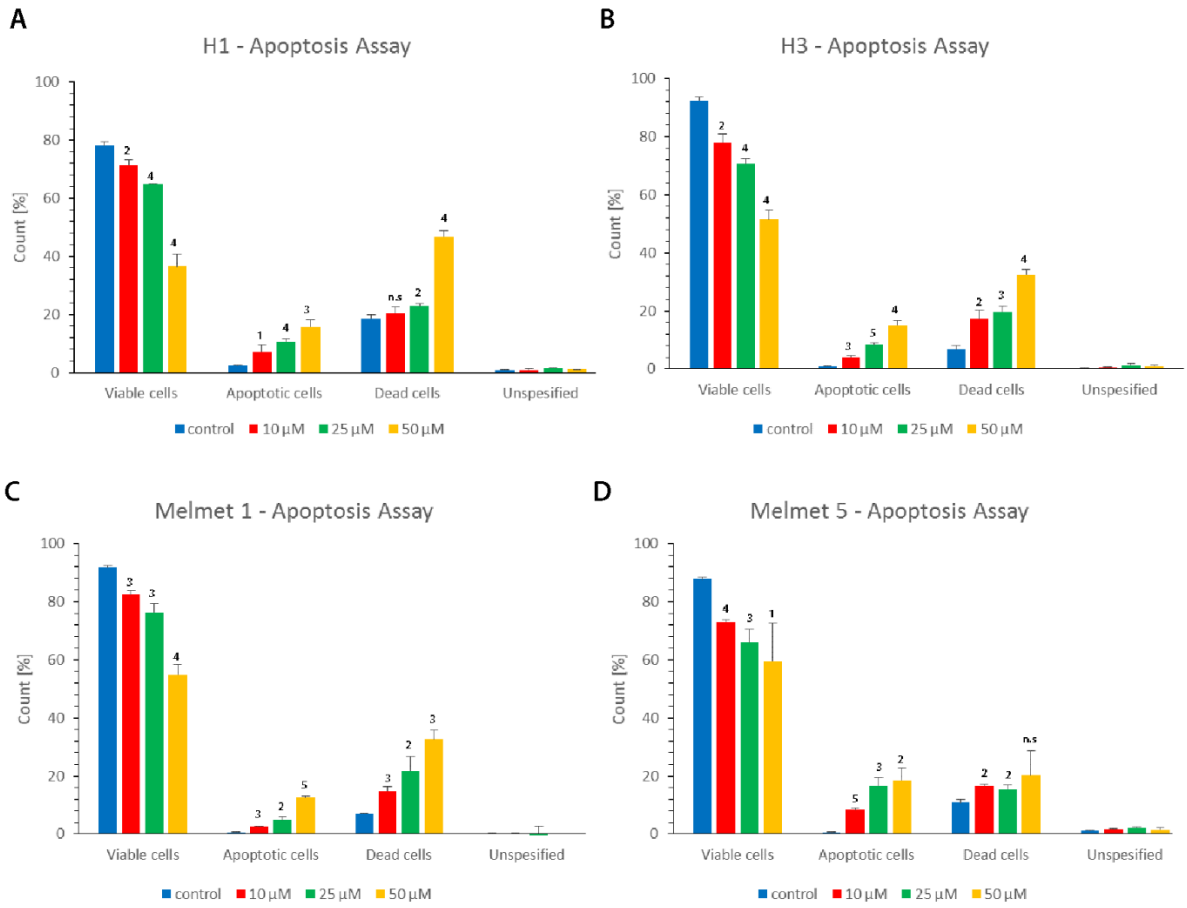

Figure 4.22 – Apoptosis assay results: For each of the four tumor cell lines: H1 (A), H3 (B), Melmet 1 (C) and Melmet 5 (D), the count of cells in the different stages (viable, apoptotic and dead cells) were compared between controls and cells treated with 10, 25 and 50 µM PJ34 for 72 hours. Three replicates were performed for each cell line, thus the graphs shows the mean value + the standard deviation of the distributions of the cells as viable, apoptotic or dead. Double sided t-test was performed for each concentration compared to the control in G_1, S and G_2M phase. n.s = not significant, 1 = $p \leq 0.05$, 2 = $p \leq 0.01$, 3 = $p \leq 0.001$, 4 = $p \leq 0.0001$, 5 = $p \leq 0.00001$, 6 = $p \leq 0.000001$.

Figure 4.22 shows that for all four cell lines increased drug dosage generally leads to decreased number of viable cell and increased number of apoptotic and dead cells.

4.4 Scratch Wound Healing Assay

A scratch wound healing assay was used to study the effect of PJ34 on cell migration and the ability to reestablish intracellular contact.

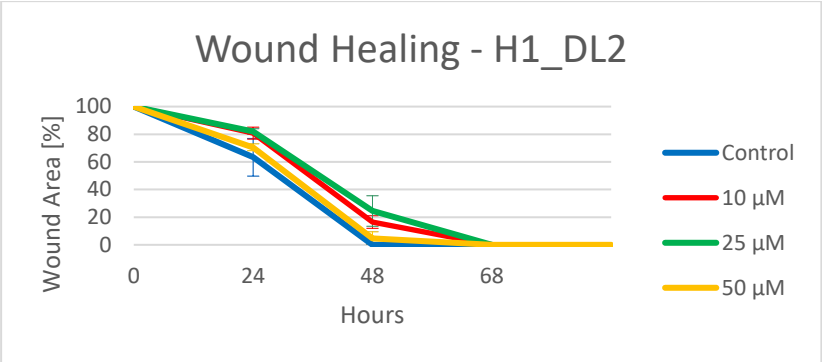

Figure 4.23 – Scratch wound healing assay for H1_DL2: The values shown in the graph consist of mean values of the wound size after 0, 24, 48 and 68 hours. The experiment was repeated three times.

One can see in the graph in figure 4.23 that the closure of the wounds occured more slowy after drug treatment, than without drug, for the H1_DL2 cell line. However, after 24 hours the only statistically significance ($p \leq 0.05$) found were between 10 µM and 25 µM, and 10 µM and 50 µM treated samples. After 48 hours the control versus 25 µM treated samples and the control versus 50 µM treated samples are still not statistically significant. However, all the other points at 48 hours were statistically significant compared to each other. After 68 hours all the wounds were closed.

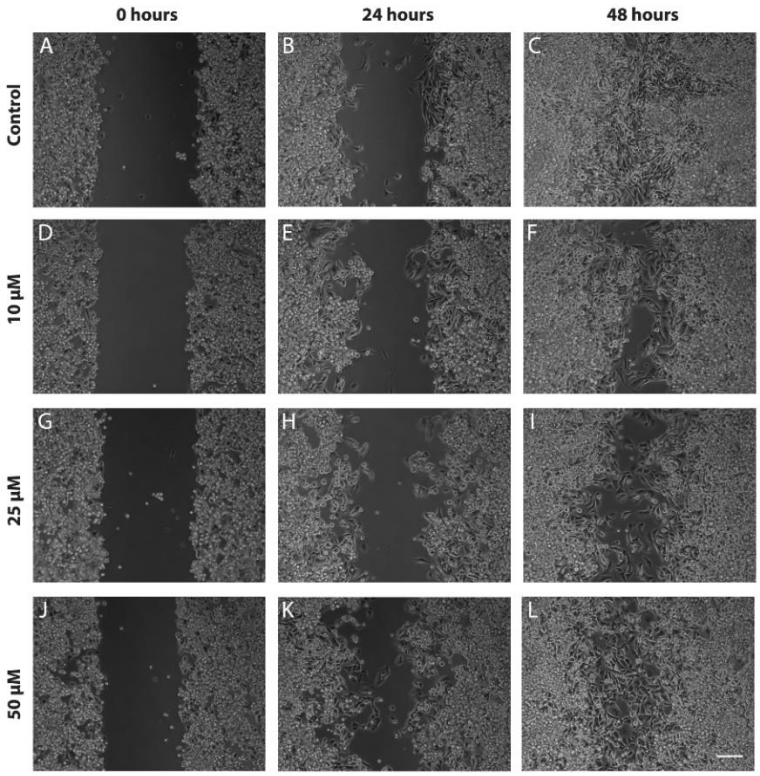

Figure 4.24 – Images from scratch wound healing assay for H1_DL2: Representative micrographs, showing the wound size closest to the mean wound size for the control (A-C) and the samples treated with 10 µM (D-F), 25 µM (G-I) and 50 µM PJ34 (J-L) after 0, 24 and 48 hours. Scale bar = 200 µm.

Figure 4.24 shows that 10 µM and 25 µM treatment slowed down the closing of the wound compared to the control.

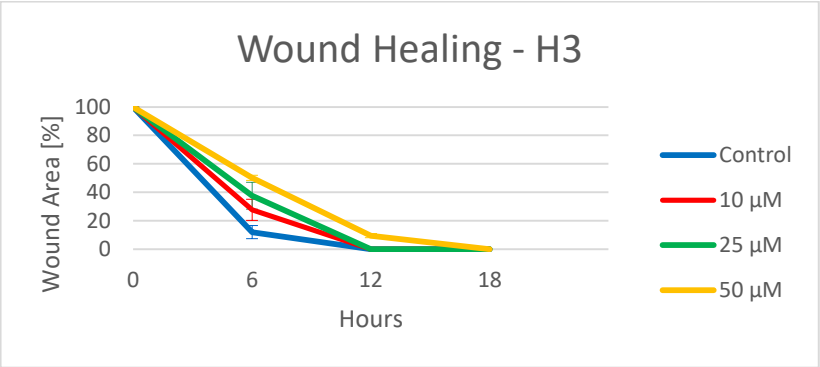

Figure 4.25 – Scratch wound healing assay for H3: The values shown in the graph consist of mean values of the wound size after 0, 6, 12 and 18 hours. The experiment was repeated three times.

Figure 4.25 shows that for the H3 cell line the higher the drug concentration, the longer time it took for the wound to close. After 6 hours, controls versus all drug doses were statistic significant ($p \leq 0.05$), as well as 10 µM versus 50 µM. This shows that the different concentrations generally were not significantly more effective compared to each other. Furthermore, the controls versus 50 µM treated samples even had a p-value lower than 0.001. After 12 hours the controls, 10 µM and 25 µM treated samples were closed. The 50 µM treated samples showed a statistically significant difference compared to all the other samples and had a p-value of ≤ 0.001. After 18 hours also the 50 µM treated samples were closed.

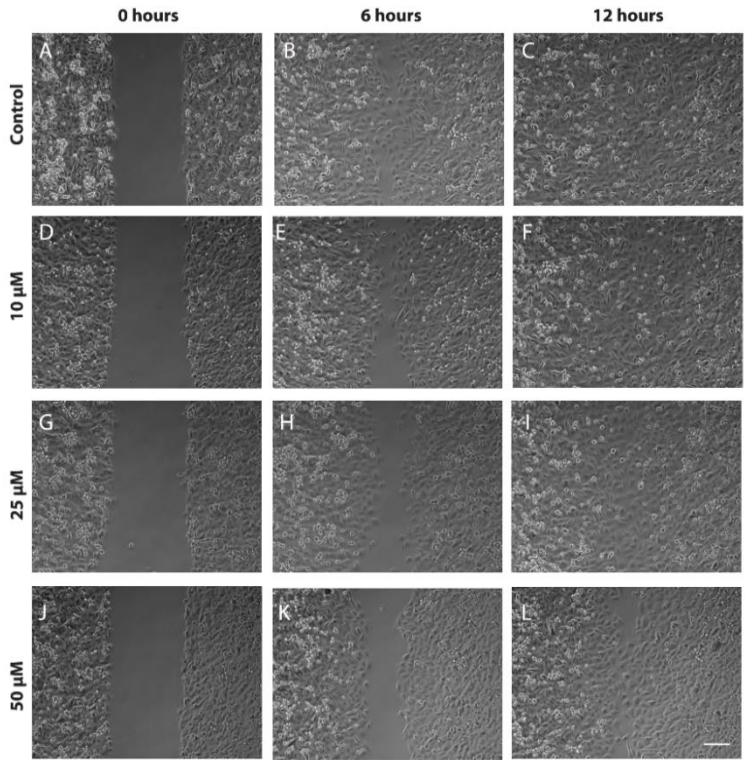

Figure 4.26 – Images from scratch wound healing assay for H3: Representative micrographs, showing the wound size closest to the mean wound size for the control (A-C) and the samples treated with 10 µM (D-F), 25 µM (G-I) and 50 µM PJ34 (J-L) after 0, 6 and 12 hours. Scale bar = 200 µm.

Figure 4.26 shows that there was a correlation between higher drug concentration and slower closing of the wounds.

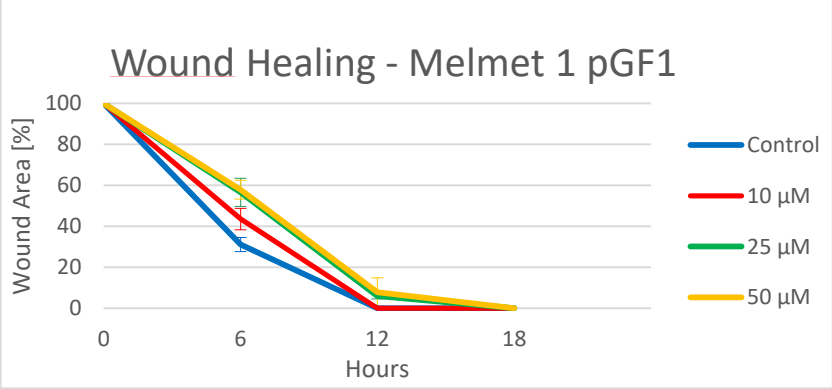

Figure 4.27 – Scratch wound healing assay for Melmet 1 pGF1: The values shown in the graph consist of mean values of the wound size after 0, 6, 12 and 18 hours. Three replicates were done.

The scratch wound healing assay done for Melmet 1 pGF1, see figure 4.27, shows that also for this cell line the drug slowed down the closing of the artificially created wounds. After 6 hours there was a statistically significant difference ($p \leq 0.05$) between the controls and all the

samples treated with different drug concentrations and between the 10 µM and 50 µM treated samples. After 12 hours both the controls and 10 µM treated samples were closed, and only the controls versus 25 µM treated samples (as well as 10 µM versus 25 µM) has a statistically significant difference. After 18 hours the last two wounds were closed.

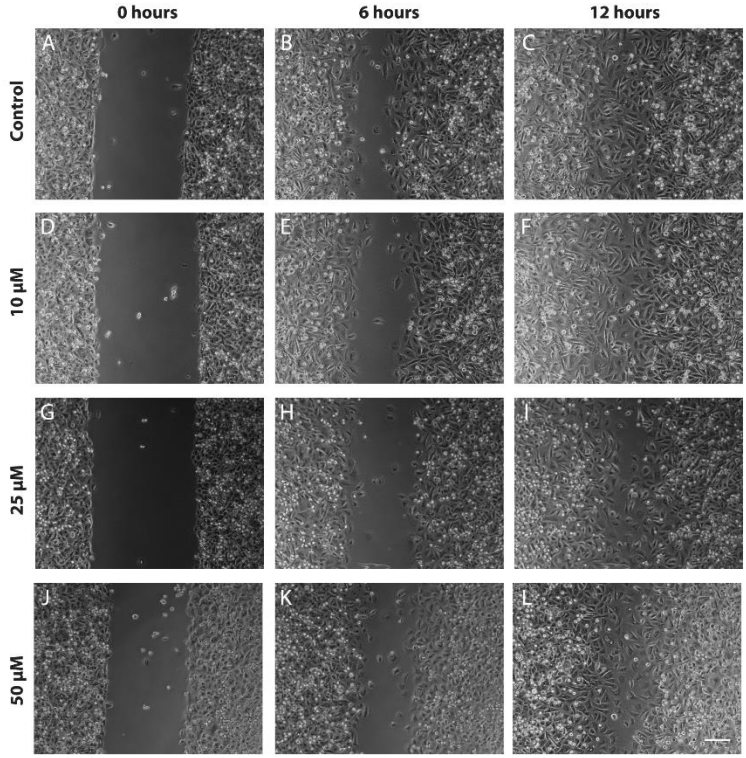

Figure 4.28 – Images from scratch wound healing assay for Melmet 1 pGF1: Representative micrographs, showing the wound size closest to the mean wound size for the control (A-C) and the samples treated with 10 µM (D-F), 25 25 µM (G-I) and 50 µM PJ34 (J-L) after 0, 6 and 12 hours. Scale bar = 200 µm.

Figure 4.28 shows demonstrate that there was a correlation between higher drug concentration and slower closing of the wounds.

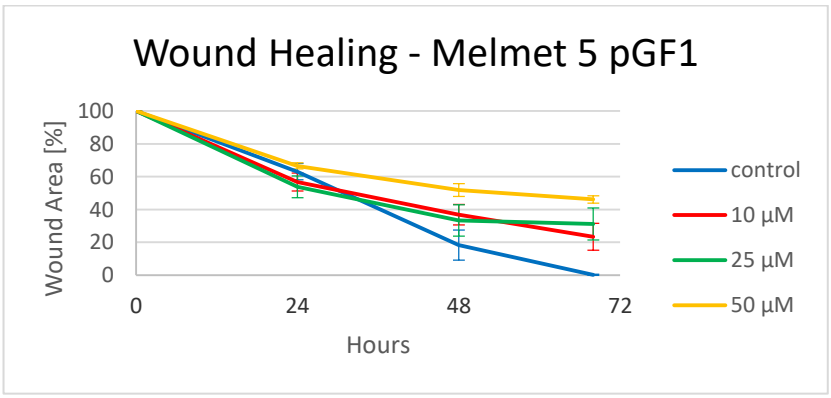

Figure 4.29 – Scratch wound healing assay for Melmet 5 pGF1: The values shown in the graph consists of mean values of the wound size after 0, 24, 48 and 68 hours. Three replicates were done.

Figure 4.29 shows the resulting graph from the wound healing assay for Melmet 5 pGF1. After 24 hours there were only a statistic significance ($p \leq 0.05$) between the controls and 50 µM treated samples and the between 25 µM and 50 µM treated samples. After 48 hours, only between the controls and 10 µM treated samples and the controls versus 50 µM treated samples there were statistic significance. However, after 68 hours all the samples compared to each other showed a statistically significant ($p \leq 0.05$) difference, except the 10 µM treated samples compared to the 25 µM treated, and the 25 µM treated compared to the 50 µM treated. In general this shows that after 68 hours there were at least a significant effect of the all the drug concentrations used on the closing of the wounds, compared to the controls.

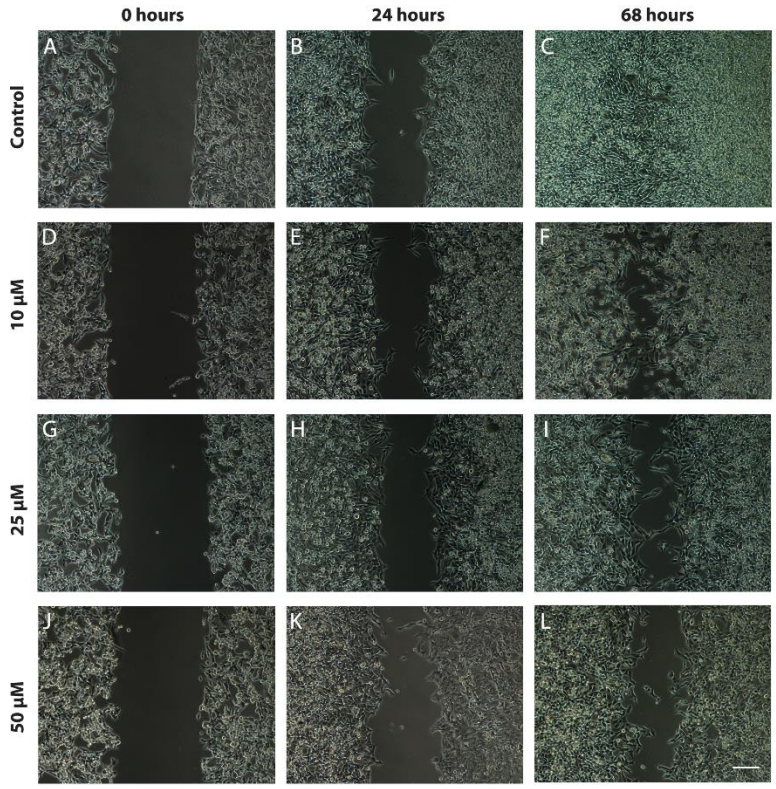

Figure 4.30 – Images from scratch wound healing assay for Melmet 5 pGF1: Representative micrographs, showing the wound size closest to the mean wound size for the control (A-C) and the samples treated with 10 µM (D-F), 25 µM (G-I) and 50 µM PJ34 (J-L) after 0, 24 and 68 hours. Scale bar = 200 µm.

Figure 4.30 show us that generally the higher dosages used of PJ34, the slower the wound closes.

To summarize, the drug slows down the closing of the wounds. In addition, the H1_DL2 and Melmet 5 pGF1 cell lines use a longer to time close the wounds in all the different samples, than the H3 and Melmet 1 pGF1 cell lines.

4.5 Western Blotting

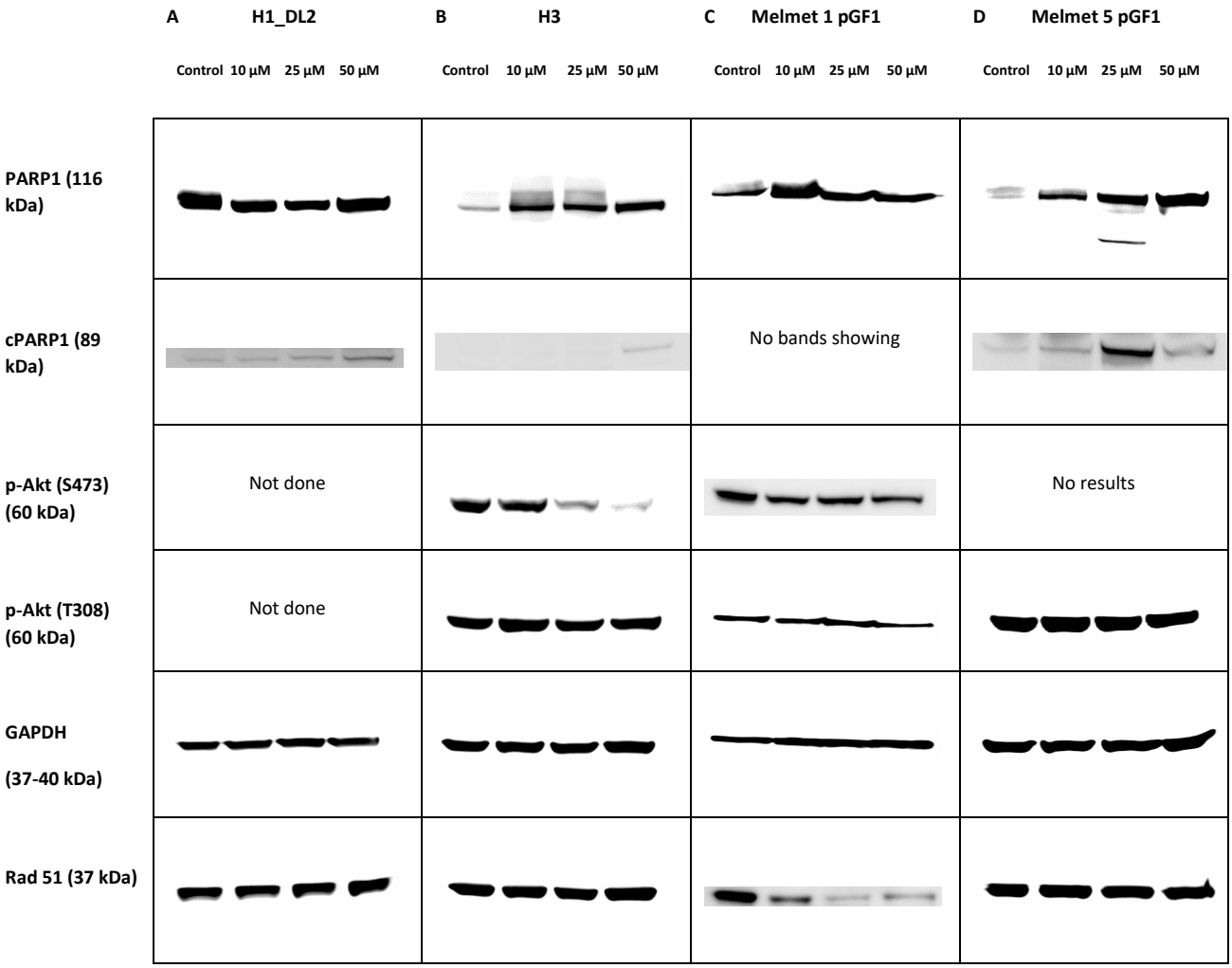

Figure 4.31 – Western Blotting results: Comparing amount of protein in control samples and samples treated with 10, 25- and 50 µM of PJ34 for all four tumor cell lines.

Figure 4.31 shows that, though PARP1 is inhibited by PJ34 in the H1_DL2 cell line, it seem that the amount of PARP1 actually increased after drug treatment in the other three cell lines. For the H1_DL2 cell line, PARP1 was inhibited increasingly after treatment with 10- and 25 µM drug. However, after treatment with 50 µM the amount of PARP1 seemed to increase, though it was still less compared to the control. For the H3 and the Melmet 5 pGF1 cell lines the amount of PARP1 increased with increasing drug dosage. For the Melmet 1 pGF1 cell line the amount of PARP1 also increased after drug tretment compared to the control, though treatment with 10 µM PJ34 increased the amount of PARP1 the most. Cleaved PARP1 was also shown to be increasing after drug treatment compared to the controls, except for in Melmet 1 pGF1, where no bands were seen. Phospho-Akt (Ser473) decreased in amount in

corresponding to higher drug concentrations for the H3 cell line and also in some degree in the Melmet 1 pGF1 cell line. The amount of Phospho-Akt (Thr308) seemed generally to not be effected by the drug, except for a slight decrease after treatment with 50 µM drug in the Melmet 5 pGF1 sample. GAPDH was used as a loading control for all the four cell lines, and the result showed a stable amount of GAPDH, as expected. Rad 51 markedly decreased in amount with higher drug concentration in the Melmet 1 pGF1 cell line. However, for the other three cell lines the amount of Rad51 protein seemed unaffected.

4.6 Spheroid Measurements

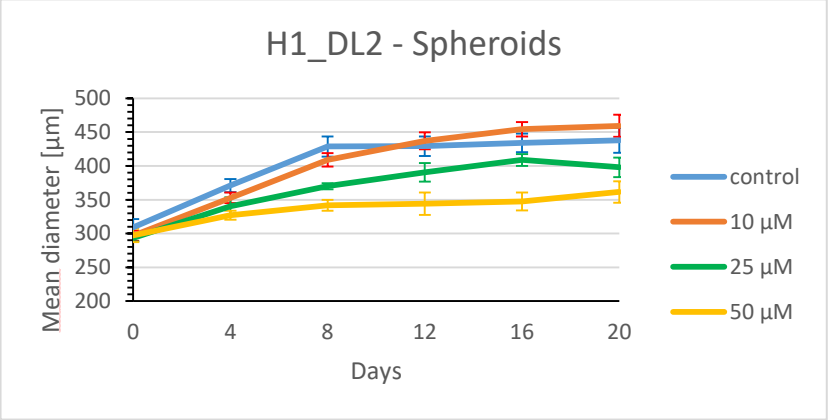

Figure 4.32 – Spheroid assay for H1_DL2: The values shown in the graph consist of mean values of the spheroid sizes after 0, 4, 8, 12, 16 and 20 days. For the control, and the ones treated with 10, 25 and 50 µM PJ34, eight spheroids were used to calculate each mean value.

Figure 4.32 shows that 25 µM and 50 µM PJ34 inhibited the growth of the H1_DL2 spheroids compared to the controls. After 20 days of treatment, all the different mean values for the spheroids had a statistically significant difference in size compared to each other. For the controls versus 10 µM treated spheroids the p-value were ≤ 0.05, for the controls versus 25 µM and 25 µM versus 50 µM treated spheroids, both p-value were ≤ 0.001. For the controls versus 50 µM, 10 µM versus 25 µM and 25 µM versus 50 µM the p-values were all $\leq$ 0.000001.

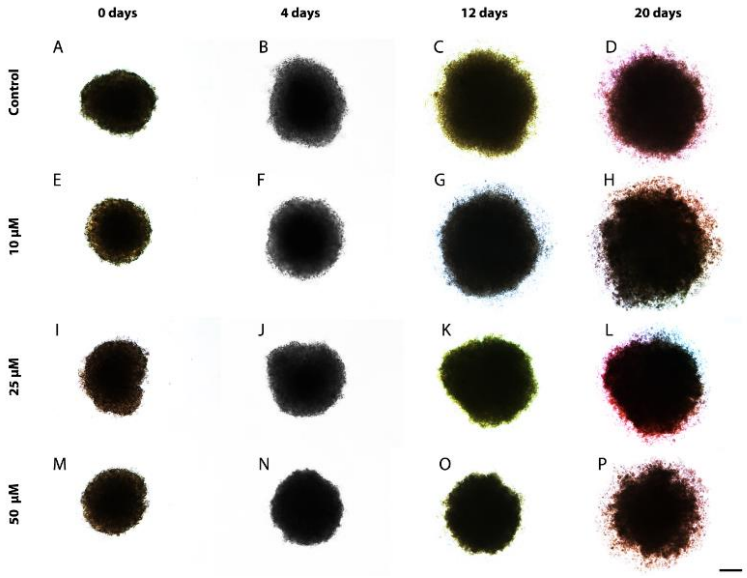

Figure 4.33 – Spheroid assay for H1_DL2, images: In this figure images after 0, 4, 12 and 20 days of the most representative spheroids for each drug concentration are followed. Scale bar = 100 µm.

Figure 4.33 shows that for drug concentrations of 25 and 50 µM PJ34 the spheroid growth was inhibited compared to the control.

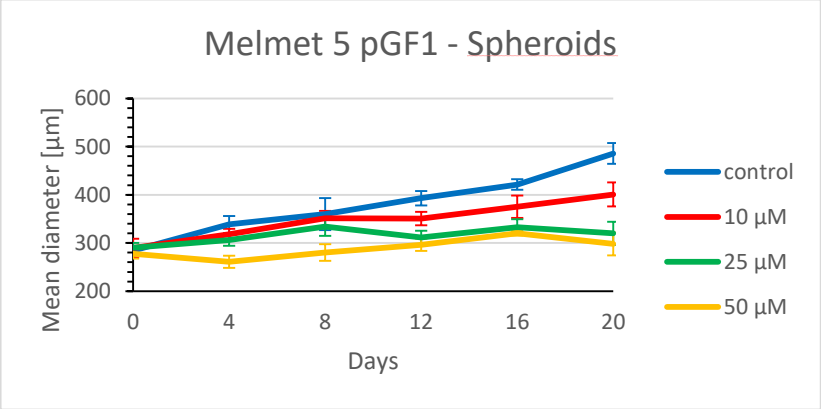

Figure 4.34 – Spheroid assay for Melmet 5 pGF1: The values shown in the graph consist of mean values of the spheroid sizes after 0, 4, 8, 12, 16 and 20. For each drug concentration, eight spheroids were used to calculate each mean value.

For the Melmet 5 pGF1 cell line, the graph in figure 4.34 shows there was a dose-dependent inhibition of spheroid growth. After 20 days, only the difference between the 25 µM treated spheroids and the 50µM treated were not statistically significant. For all the other different concentrations (control, 10, 25- and 50 µM treated) there were statistically significances between each of them (p-value ≤ 0.00001).

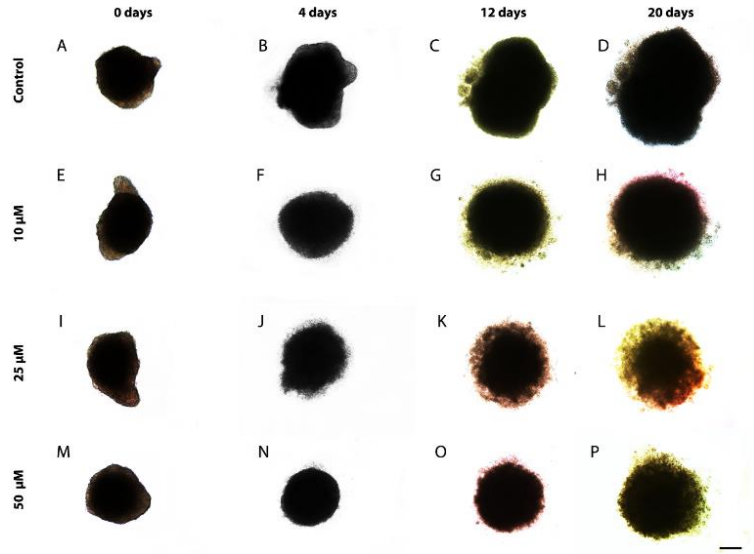

Figure 4.35 – Spheroid assay for Melmet 5 pGF1, images: In this figure images after 0, 4, 12 and 20 days of the most representative spheroids for each drug concentration are followed. Scale bar = 100 µm.

Figure 4.35 shows that the higher the drug concentration, the slower the spheroids grew compared to the untreated spheroids.

The remaining two cell lines, H3 and Melmet 1 pGF1 would not form proper spheroids, and therefore, this assay could not be performed on these cell lines.

4.7 In Vivo

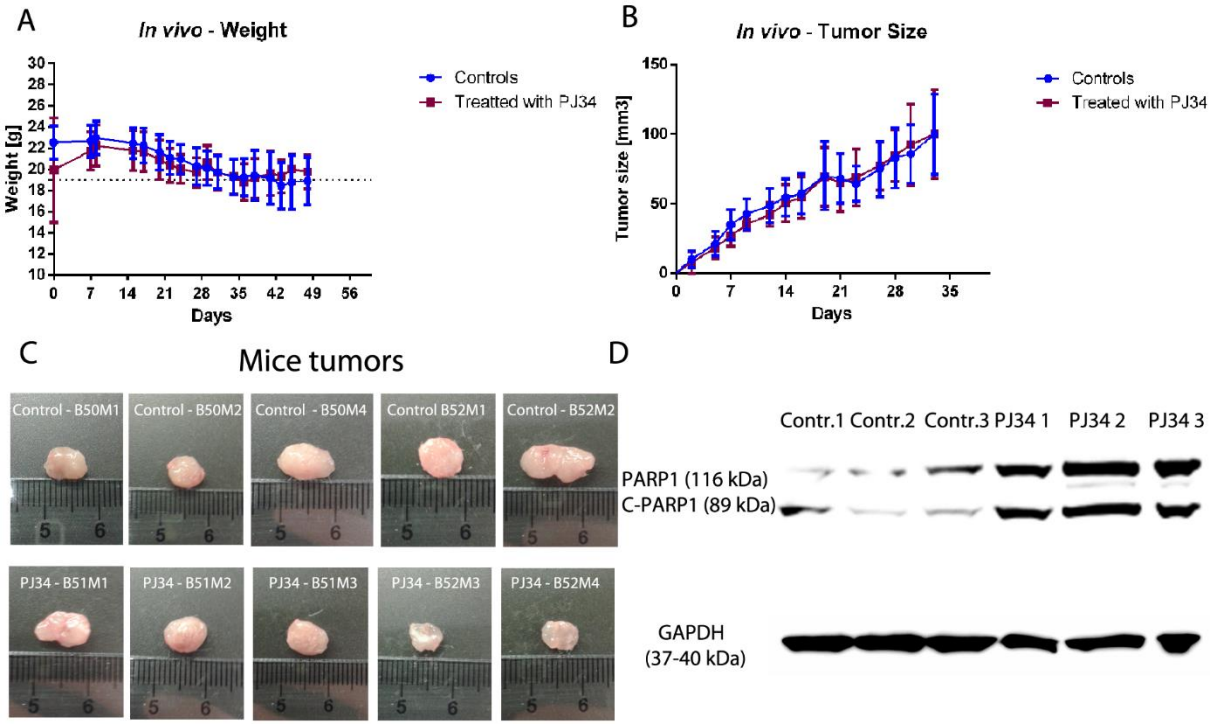

Figure 4.36 – *In vivo* results: The figure shows the mean value for weight (A) and tumor size (B) through the experimental period for both the control mice and the ones treated with PJ34. The figure also shows pictures of all the tumors (C), after being removed from the mice (a ruler is used as a scale). And lastly, the figure shows western blotting from three control tumors and three treated tumors (D). The western blots shows the amount of PARP1 protein and cleaved-PARP1 protein in the respective samples, and GAPDH is used as a loading control.

Figure 4.36 shows the results from the *in vivo* experiment. The mean weight of the control-animals did not differ from the weight of the animals treated with PJ34. As seen in the images in figure 4.35 C the individual tumor sizes differed from each other, but as shown in the graph in figure 4.35 B, the mean tumor size did not change between the control group and the treated group. In figure 4.35 D the results of the western blotting done on three of the control tumors (B50M1, B50M2 and B50M4) and three of the tumors treated with drug (B51M1, B51M2 and B51M3) are shown. The western blot clearly shows that the amount of both PARP1 and cleaved PARP1 was higher in the tumors treated with drug than the control tumors. GAPDH showed fairly stable amount throughout the different samples.

5 Discussion

For patients with metastatic melanoma the 10-year survival rate is less than 10%. There is an eminent need for successful new therapies for metastatic melanoma. Attempts to improve the survival have generally failed (10). Furthermore, counting all cancers, melanoma has the highest tendency to metastasize to the brain (79). Brain metastases are found in around 50% of the patients with advanced melanoma (26). In addition, patients often acquire multiple brain metastases, which is associated with a poor prognosis (79).

For successful treatment of brain metastases the therapeutic drug has to reach the brain, and thus cross the blood-brain barrier (BBB) (80). If a drug is to cross the BBB, the molecular weight has to be below 400 – 500 Da, and the compound must be lipid soluble (43). The drug used in this thesis, PJ34, has a molecular weight of 331.8 Da, and previous studies show that PJ34 is able to cross an intact BBB (59, 64). PJ34 is a novel potent specific inhibitor of PARP1 (57). PARP1 is a nuclear enzyme with key functions regarding cellular responses to DNA damage and DNA repair as well as regulation of transcription, cell death, cell proliferation and cell cycle (47, 57). Expression of PARP1 is found to be overexpressed in several malignancies, including melanoma (47). Furthermore, PARP inhibitors are an important, though still emerging, class of anticancer drugs. Therefore, it is important to elucidate the underlying mechanisms by which PARP1 inhibitors function in tumor cell biology (46).

5.1 Cell Viability Assays

In the monolayer viability assays, a dose dependent drug inhibition was shown for all four tumor cell lines. The mean IC_{50} doses were in the 10^{-6} M range, while the mean IC_{50} dose for the fibroblast cell line, SV80, was in the 10^{-5} M range (figures 4.1, 4.2) The results from the soft agar viability assays (figure 4.3) were similar to the monolayer results. The viability graphs showed a sigmoidal shape with a correlation between increased drug dosage and decreased cell viability. It is acknowledged that the 3D environment in soft agar assays mimics more closely the environment seen in vivo. The soft agar assay measures the cells ability to grow in suspension in a semi-solid agarose gel (81).

Chevanne and colleagues reported that 10 mM PJ34 led to a severe block of cell proliferation, associated with cell death,- for human M14 melanoma skin metastatic cells (82). In this article trypan blue staining followed by counting in a Burker chamber was used to determine the viability and the number of cells (82). In the current thesis, 100 µM of PJ34 inhibited cell viability for almost all for the cells after 72 hours. These results indicate that PJ34 is more effective on the melanoma cells *in vitro* in this thesis compared to the M14 melanoma cells.

Furthermore, Gangopadhyay and colleagues found that treatment with 30 µM PJ34 for 72 hours eradicated the human metastatic lung cancer cell lines Calu-6, A549 and H460 by 60.7% ± 4.6, 48.3% ± 7.1, and 40.2% ± 5.8 respectively (58). This was demonstrated by the use of a WST dye assay. The mean IC_{50} doses for these lung cancer cell lines were approximately 30 µM, indicating that a dosage 10 times higher than used in this thesis (see table 4.1) was necessary to kill 50% of the cells. In addition, they found that PJ34 had little effect on normal lung epithelium (HBEC cells) (58). The drug effect found on the fibroblast cell line in this thesis was more substantial (around 10^{-5} M). However, the tumor cell lines needed a 10 times lower dose to kill 50 % of the cells than the fibroblasts cell line. This still establish a therapeutic window that can be utilized in further experiments. By the use of light microscopy we confirmed that the decrease in viability in all the four tumor cell lines as well as the fibroblast cell line, was in fact due to cell death.

It has previously been demonstrated that after 48 hours of treatment with 10 µM PJ34, more than 99% of the cells from the human breast cancer cell line, MCF-7 were eradicated. For the human breast cancer cell line, MDA-MB-231, 72-96 hours of treatment with 20-30 µM PJ34 led to obliteration (83). Furthermore, PJ34 has been shown to inhibit the growth of human liver cancer cell lines (HepG2 and SMMC7721) and human multiple myeloma (RPMI8226 cell line), and to have potent anti-proliferating effects against human leukemia cell lines (ATLL and HTLV-I-transformed) and human ovarian cancer epithelial cells (C13* cell line) (57, 63, 84, 85). As previous studies have to a little degree focused on metastatic melanoma, this underlines the need for further examination of PJ34 as a potential anti-cancer drug for melanoma metastases, especially metastases to the brain.

5.2 DNA Cell Cycle Analysis

The main trend in the DNA analysis showed an increased percent of cells in the G_2M phase and to some degree a simultaneously decrease in G_1 phase after treatment. However, this shift was not especially prominent or consistent throughout the different cell cycle experiments.

There are several checkpoints between the different phases of the cell cycle. At a checkpoint in the end of G_1, cell cycle arrest will follow if the DNA is damaged. Arresting cells in late G_2 phase is a response to damaged DNA or not fully replicated DNA. Furthermore, the checkpoint in M phase leads to arrest of mitosis if the daughter chromosomes are improperly aligned (86).

It has previously been shown that PJ34 can cause cell cycle arrest in leukemia, breast cancer (MCF7) and melanoma (M14) cell lines (87, 88). Madison and co-workers demonstrated that PJ34 caused a dose-dependent G_2M growth arrest in HeLa (cervical cancer) and H1299 (lung carcinoma) cell lines (87). Madison and colleagues also found that that mitotic growth arrest mediated by PJ34 was not necessarily PARP 1 and 2 dependent. The G_2M arrest was p21 dependent, however, the p21 activation was also not exclusively PARP1 or 2 dependent. They found that both p53(Ser15) and Chk1(Ser345) were phosphorylated and p53 was activated. However, p53, Chk and ATM were not necessary for mitotic arrest. Madison et al suggested that there was an ATM/ATR cross talk and a direct activation of ATR-Chk1 or ATM-Chk2, which initiated and maintained the mitotic arrest. Moreover, they suggested the possibility that there might be an ATM/ATR dependent, Chk1/2 and p53 independent target, or there were separable PARP dependent and PARP independent effects on p21 activation and the checkpoint cascade (87). It would also be interesting to investigate whether or not the mitotic arrest in our tumor cell lines is dependent on PARP1 and PARP2.

Most human cancer cells have extra centrosomes (61). For normal bipolar spindle formation and accurate chromosome segregation in cells during mitosis, it is essential with a bipolar assembly of the centrosomes. Cancer cells have often developed a molecular mechanism where they cluster their extra centrosomes at two poles, and thus imitating mitosis in normal cells. PJ34 may interfere with this bipolar clustering. If this bipolar clustering is not

accomplished, multipolar spindle structures will form and cause aberrant chromosome segregation. This will again prevent normal cell division, leading to G_2M arrest and subsequent cell death. However, the molecular mechanisms leading to cell death after unsuccessful accomplishment of mitosis, are poorly understood (61, 62).

Castiel and colleagues found that PJ34 caused G_2M transitional arrest in the cell cycle of both the MDA-MB-231 (mammary cancer) and the MCF-10 (normal mammary epithelia) cell lines. The G_2M arrest was permanent and followed by massive cell death, while the normal epithelial cells overcame the arrest and continued normal proliferation. Normal mesenchymal cells and Huvec cells (endothelial cells from human umbilical vein), were also shown to be resistant to the cytotoxic effect of PJ34. It was shown that PJ34 did not prevent bipolar assembly of centrosomes, formation of a bifocal spindle, nor did the compound affect chromosome segregation. This indicated that PJ34 did not affect the cell cycle in these normal human cell lines (61). Castiel and colleagues also found that in cells containing supernumerary centrosomes, PJ34 acts as a centrosome de-clustering agent. As mentioned, in most human cancers supernumerary centrosomes within the tumor cells are very common, while the number of centrosomes is restricted to two per cell in normal somatic cells (accomplished through several control mechanisms) (61, 62). One possible effect of PJ34 is thus that it may cause G_2M arrest because of its interference with bipolar clustering in cells with extra centrosomes. The fact that oncogenic $BRAF^{V600E}$ induces supernumerary centrosomes in human melanocytic cells, as well as spindle abnormalities and aneuploidy, support this theory for our cell lines (89). In addition, the $BRAF^{V600E}$ mutation is found in more than 60% of melanomas, including the H1_DL2 cell line used in this thesis (26).

Castiel and colleagues also tested PJ34 on colon (DLD-1), ovarian (HeyA8), lung (H1299) and pancreatic (Panc-1) tumor cell lines, and found that PJ34 obliterated the cancer cells in a similar way as for the mammary cancer cell line MDA-MB-231. Furthermore, they discovered that 20-30 µM of PJ34 lead to G_2M arrest in these cells followed by massive cell death after 48-96 hours of treatment. In these cells, PJ34 prevented the bipolar clustering of the cells with supernumerary centrosomes. This resulted in aberrant alignment of chromosomes and multipolar spindles after 18 hours of treatment. A significant correlation was found between the number of cells with multipolar spindles and the decrease in cell

viability (61). The exclusive cytotoxic effect of PJ34 in cells containing more than two centrosomes, imply that it may be used as a selective chemotherapy in many human cancers (61, 62).

Taking the results from literature together, it may then be possible that the result observed in our work could be caused by G_2M arrest following a PJ34 de-clustering effect. Due to time constraints, we have not been able to study whether or not supernumerary centrosomes played a role in the effects of PJ34 seen in the current work.

5.3 Apoptosis Assay

The results regarding apoptosis clearly showed for all four cell lines that increased concentration of PJ34 increased the percentage of apoptotic cells, and simultaneously reduced the percentages of viable cells. In addition, the number of dead cells generally increased with increasing drug dose.

There are contradicting results in literature on the apoptotic effects of PJ34. Xiong and colleagues found that 60 µM PJ34 alone did not increase the percentage of apoptotic cells in the human multiple myeloma cells (RPMI8226 cell line) after treatment. However, when PJ34 was used in collaboration with the chemotherapeutic alkylating agent Melphalan the apoptosis percentage increased, compared to using Melphalan alone. Melphalan results in single or double stranded breaks in the DNA. If not repaired, these breaks will cause mutations and genomic instability which leads to cell death (84). As previously mentioned in this thesis, PARP enzymes repair single stranded breaks, and PJ34 act as a PARP inhibitor (57).

Death by apoptosis of the human melanoma cell line, M14, was excluded by Chevanne and co-workers following treatment for 24 hours by 10 µM PJ34 (82). This lack of effective results may be due to the usage of a low drug dosage, in addition to merely 24 hours of treatment. In this thesis, a statistically significant increase in apoptotic cells after treatment with merely 10 µM PJ34 were seen for all four tumor cell lines, when treated for 72 hours.

Supporting our findings, Bai et al showed that treatment with 25 µM PJ34 for 72 hours induced apoptosis in all the patient derived ATL-like cell lines (an aggressive type of peripheral T-cell leukemia) and most of the HTLV-1-transformed (Human T-cell leukemia virus type I) cell lines (63).

Furthermore, PJ34 was also found to induce apoptosis in different lung cancer cell lines by Gangopadhyay and colleagues. Apoptosis was induced in the lung adenocarcinoma cell line, Clu-6, which possess defects in genes related to DNA repair in the BRCA-FA pathway. In addition, apoptosis was induced in the lung cancer cell lines A549 and H460, were no reports of defective DNA repair have been found. PJ34 is normally utilized when patients harbor mutations in BRCA1 or BRCA2, or mutations in other DNA repair gens. However, the results by Gangopadhyay and colleagues, shows that PJ34 can be used against cancers not carrying a BRCA mutation as well (58).

5.4 Scratch Wound Healing Assay

The results from the scratch wound assay in general displayed that there was a dose-dependent inhibition of wound closure. However, H1_DL2 cells treated with 50 µM drug showed no significant difference in the closing rate of the wound at 24 or 48 hours, compared to untreated cells.

Rodriguez and colleagues showed that treatment of the murine malignant melanoma cell line B16-F10 with similar doses of PJ34 (10 µM), as used in our work, decreased the cell migration and thereby decreased the wound closing *in vitro* (46). Moreover, in our work, wounds made in confluent cultures from the H3 and Melmet 1 pGF1 cell lines closed more rapidly than the remaining two melanoma cell lines (18 hours vs 68 hours). These differences might be explained by the findings of Nygaard and co-workers. They found that Melmet 1 and Melmet 5 exhibited different phenotypes. The Melmet 1 cell line had a lower degree of proliferation than the Melmet 5 cell line. However, the Melmet 1 cell line was considered to be invasive, while the Melmet 5 cell line seemed to have a non-invading phenotype (37). The explanation of the different wound closing times might be applied to all our cell lines, as we

know from unpublished experiments in our lab that the H3 cells are less proliferative than the H1_DL2 cell line.

Interestingly, El-Hamoly and colleagues found that in their mouse model of excision wounding that PARP inhibitors, among them, PJ34, actually accelerate wound closing. Wounds in PARP1 knockout mice also healed faster than in the wild type mice. In addition, *in vitro* scratch assays showed that 10 µM PJ34 treatment resulted in a significantly faster migration and wound closing of primary human keratinocytes. They suggested that PARylation by PARP1 activation resulted in delayed wound healing. This means that by using a PARP1 inhibitor the wound healing would be accelerated. PARylation is a covalent modification of proteins performed by PARP enzymes (90). Zhou and colleagues also obtained similar results as El-Hamoly et al. First, they observed that there was a significant increase in PARP activity under ischemic and diabetic conditions, which in turn correlated with slower wound healing and migration of HUVEC cells. PARP inhibition by PJ34 accelerated wound closing both in animal -and in *in vitro* models by promoting angiogenesis (91).

The reason for these conflicting results is not clear. Maybe PJ34 have opposite effects on cancerous and non-cancerous cells. Further, the delay in wound closing time seen in this work may not be caused by inhibition of PARP1 but by an increase of PARP1, see western blotting results in subchapter 4.4 and the discussion in subchapter 5.5.

5.5 Western blotting (WB)

The WB results showed that while PARP1 was inhibited for the H1_DL2 cell line, in general, the amount of PARP1 actually increased after treatment with PJ34. The amount of cleaved PARP1 also increased after drug treatment, compared to the untreated controls. Furthermore, the amount of phospho-Akt (Ser473) decreased in the H3 cell line when treated with 25 µM and 50 µM of PJ34. In addition, a small decrease in phosphor-Akt (Ser473) with increasing drug dose, was also seen for the Melmet 1 pGF1 cell line. The amount of phospho-Akt (Thr308) was generally not affected by the drug. Rad51 decreased in amount with higher drug

concentration in the Melmet 1 pGF1 cell line. However, for the other three cell lines the Rad51 protein seemed unaffected.

Bai and colleagues found by WB, that HTLV-I transformed leukemia cell lines MT2, MT4 and C91PL exhibited a decreased amount of PARP1 after treatment with PJ34 (63). In coherence with these findings, Wang et al also discovered that PJ34 downregulated PARP1, as PARP1 significantly decreased with increasing dose of PJ34 in the ovarian cancer cell line C13* (85). Contrary to this, PARP1 was upregulated after treatment in our work. Wang and co-workers used drug dosages in the mM area instead of µM (which we used), which may explain the differences observed. An alternate explanation could be that the viable cells on which the WB was performed might be resistant to PARP1 inhibition. We removed the apoptotic cells floating in the medium before preparing the cell lysate, and these cells might have died as a result of PARP1 inhibition. Therefore, a western blot on the apoptotic cells might have shown a decreased amount of PARP1.

Yet another explanation could be that our cell lines were exposed to excessive stress related to drug treatment and thus responded by an overcompensating mechanism, namely a biphasic response, resulting in over-production of PARP1. Further studies on this would be warranted. The term biphasic response (hormesis) is used to describe the overcompensatory response to a disruption in homeostasis (92). A biphasic response can be seen at low doses of a chemical were large disruptions in homeostasis are not able to mask this response. In addition, this normally gives an effect opposite to the one found at higher doses of the same chemical. Higher doses will overcome the compensatory abilities and a standard dose-response relationship occurs, see figure 5.1. This means a higher dose of PJ34 could have shown inhibition of PARP1. In addition, since the amount of PARP1 generally increased with increasing drug dosage the, this might indicate that the drug doses were at the downward slope of the biphasic response (see figure 5.1, II – hormesis) (92).

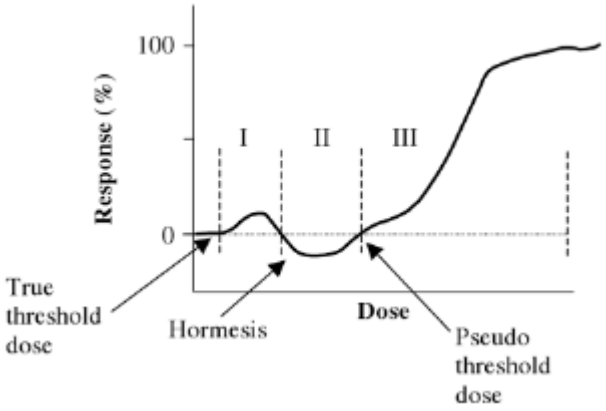

Figure 5.1 – Biphasic response (= hormesis): The figure shows how overcompensation can lead to an opposite response than what one would expect. Reprinted from (92).

The observation that the amount of cleaved PARP1 generally increased with increasing drug dose may indicate that with increasing drug dose the DNA damage exceeds the cells repair capacity. This means that there is a shortage of functioning PARP1 (93). Since the amount of cleaved PAPR1 seemed to increase with increasing drug dose, this may suggest that PJ34 still had some inhibitory effect on PARP1. Furthermore, Xiong and colleagues found that after treatment with 60 µM PJ34 for 24 hours, Rad51 was downregulated in the human multiple myeloma cell line RPMI8226 (55). These findings coincide with the results for the Melmet 1 pGF1 cell line. Rad51 is essential for homologous recombination and repair of double stranded breaks in the DNA (94, 95). High expression of Rad51 in cancer has been suggested to correlate with enhanced invasiveness and aggressiveness of tumor cells, in addition to a poor prognosis and resistance to chemotherapeutic DNA-damage. Consequently, targeting of Rad51 has been presented as a possible anti-cancer treatment. Additionally, it has been show that downregulation of Rad51 can increase the sensitivity of human cancer cells to chemotherapy, relative to normal cells (95). This means that the downregulation of Rad51 might in some part be responsible for the anti-cancerous effect of PJ34 on Melmet 1 pGF1. By demonstrating that PJ34 can inhibit Rad51, its potential use in cancer therapy may also be broadened.

Moreover, Wang et al found that after treatment with 15 µM PJ34 for 24 hours, the amount of phospho-Akt (S473) deceased in the human osteosarcoma cell line U2OS and the non-small cell lung cancer cell line H358. The decrease in phospho-Akt (S473) was found in the H3 cell

line and to some extent in the Melmet 1 pGF1 cell line. This might indicate that some of the anti-cancer effect that PJ34 has on these cell lines may be caused by attenuation of the Akt-FOXO3A pathway (96). More importantly is the possibility that PJ34 exerts its effects through the PI3K-Akt pathway, due to its inhibition of Akt. The PI3K pathway might play an important role in the development of aggressive melanoma tumors. Additionally, previous studies have shown PI3K pathway activity to increase in melanoma (26, 97). Other studies have also shown that inhibition of PARP1, activates the PI3K-Akt pathway (98). Since we found that the amount of PARP1 was increased after PJ34 treatment, these results could further indicate that PJ34 might actually inhibit the PI3K-Akt pathway. Furthermore, it may be because of this inhibition, that PJ34 has an inhibitory effect on our metastatic melanoma cell lines as well.

5.6 Spheroid Measurements

The results from the spheroid measurement of the H1_DL2 and the Melmet 5 pGF1 cell lines showed that there was a dose-dependent inhibition of tumor spheroid growth after treatment with PJ34.

No previous studies on the effect of PJ34 on tumor spheroids *in vitro* could be found. However, there is an astonishing amount of evidence that compared to simple two-dimensional cell monolayers, three-dimensional cell cultures portrays more accurately the complexity of the *in vivo* tumor microenvironment (77, 99-104). The tissue construction and the extracellular matrix, influence the tumor cells responses to signals in their microenvironment (77). Thus, three-dimensional cultures more accurately demonstrate the *in vivo* tumor microenvironment regarding cellular heterogeneity, pH, oxygen- and nutrient gradients, cell-cell interactions, gene expression profiles and matrix deposition (77, 99, 103). Several models of *in vitro* solid tumors have been established, though the multicellular spheroid model is one of the best explored and most frequently used. It has also been shown that the ultra-low attachment 96-well round-bottomed plate (as used in this thesis) is the best method of generating the most reproducible spheroids, compared to other techniques, e.g. using the agar-coated 96-well plates (77).

For a cancer treatment to be effective, the drug must reach all tumor cells. If one tumor cell survive it could regenerate the entire tumor (104). Hypoxia or poor vascularization within the spheroids can limit the accessibility of cytotoxic agents, as is seen in solid tumors. This illustrate that spheroids are more eligible for studying drug penetration than monolayer cultured cells (99). In addition, the cells in a solid tumor are exposed to a large gradient of concentration as the drug diffuses from blood vessels, as well as being subject to different microenvironments. On the contrary, cells in monolayer are in general exposed to a uniform concentration of drug and an invariable environment (104).

Based on all the statements described above, the fact than PJ34 inhibits the growth of tumor spheroids *in vitro* is of great importance. As mentioned, the results from the 3D spheroids give us a more realistic view than the monolayer assays of the results that could be expected *in vivo*. We did not perform any more spheroids assays, like for instance WB on spheroids. Due to time constraints, we prioritized doing WB on the *in vivo* tumors, as we regard this to have more clinical relevance.

5.7 In Vivo

The result from our *in vivo* experiment showed that the drug did not have any effect on the tumor size, nor the weight of the mice, when administering 10 mg/kg PJ34 intraperitoneally three times a week.

Huang et al found that tumors from the human liver cancer cell line, HepG2, were inhibited by PJ34, when grown in nude mice. They injected 2 000 000 HepG2 cells into the bilateral flanks of the mice, and after two weeks tumors formed. The mice in the treatment group were injected intraperitoneally every other day with 100 µL of 3 mg/kg PJ34. The mice in the control group were injected with saline with the same volume and interval as the drug treated group. The injections continued for 21 days. The results showed a significant tumor reduction for PJ34 treated mice, compared to the untreated mice ($P < 0.05$). Therefore, Huang and colleagues concluded that PJ34 alone was able to inhibit HepG2-derived tumor growth in nude mice (57).

Inbar-Rozensal and colleagues found that the development of human breast cancer (MCF-7 and MDA-MB-231 cell lines) xenotransplants in nude mice were prevented by PJ34. 2 mM PJ34 in 100 µL PBS was inserted into implanted subcutaneous osmotic pumps. This ensured a constant and slow release of PJ34 (about 0.6 nmol/h) in a course of two weeks. In the control mice, pumps were not implanted, or the pumps contained only PBS. 24 hours later 10 000 000 breast cancer cells were injected subcutaneously, adjacent to the osmotic pumps. In control mice injected with MDA-MB-231 cells, tumors developed within 10 days. For the control mice injected with MCF-7 tumors developed within 6-7 weeks. Unlike the controls, no visible tumors emerged during 10 weeks after injection with MDA-MB-231 cells, or during the 4 months after injections of MCF-7 cells (83). The results from this experiment suggests that pretreatment of animals before tumor cell injections may prevent the onset of tumor growth. It would therefore be of interest to us to perform similar studies, by injecting the H1_DL2 cells subcutaneously after pretreatment.

There were several differences in Huangs and Inbar-Rozensals studies, compared to the *in vivo* experiment performed in this thesis, which could explain the differences in tumor growth observed. We used human, metastatic melanoma cells (as opposed to liver cancer or breast cancer cells), and a different dosage scheme. The dosage used in our work was 10 mg/kg for the first three weeks, following 30 mg/kg for the next two weeks. In comparison, Huang et al used a dosage of 3 mg/kg for three weeks, while Inbar-Rozensal delivered the drug using osmotic pumps (57, 83). Further, different amounts of tumor cells were inoculated. In addition, it could be that delivery of drug through the blood stream is more efficient to tumors residing in the flank area than the ones growing subcutaneously in the neck area, due to possible differences in tumor vascularization. Further studies injecting the H1_DL2 cells subcutaneously after pretreatment should be performed, as well as optimizing tumor cell load/injections and dosage schemes. It would be of particular interest to see if pretreatment of animals prior to tumor cell injections would lead to tumor growth inhibition. If successful, this would also be relevant in a clinical setting, for instance as a preventive treatment of cancer patients with advanced disease, before these patients show tumor spread to the brain.

The WB done on the *in vivo* tumors showed that the amount of both PARP1 and cleaved PARP1 were higher in the tumors treated with drug than the control tumors. The increased

amount of PARP1 was consistent with the increased amount of PARP1 found in *in vitro* on H3, Melmet 1 pGF1 and the Melmet 5 pGF1 cell lines. On the contrary, in the H1_DL2 cell line PARP1 was inhibited for the two lowest drug doses, though the amount of PARP1 after treatment with the highest drug dose was similar to the control. The results showing the increased amount of PARP1 after PJ34 treatment *in vivo*, may be due to the same overcompensation mechanisms as described in subchapter 5.5, see figure 5.1. The increased amount of cleaved PARP1 was consistent with the results from our *in vitro* studies on the H1_DL2 cell line. As mentioned in subchapter 5.5, the increased amount of cleaved PARP1 suggests that the DNA damage exceeds the cells repair capacity (93). In the *in vivo* results, the increased amount of cleaved PARP1 in the treated tumors compared to the control tumors were very prominent. Though PJ34 seemed to increase the amount of PARP1, this may mean that the drug still had an inhibitory effect on some of the PARP1 enzymes.

5.8 Summary and Conclusion

In compliance with findings in literature, PJ34 was demonstrated to have a dose dependent inhibitory effect on cell viability on all four tumor cell lines, both in 2D and 3D cell culture assays. DNA Assay generally showed a shift from G_1 to G_2M, however, not especially prominent or consistent throughout the different cell cycle experiments. Even so, this might still suggest that PJ34 can cause a G_2M arrest in our metastatic melanoma cell lines, also in accordance with previous studies. G_2M arrest may possibly be mediated by PJ34 actions as a centrosome de-clustering agent, although this was not studied in this thesis. The apoptosis assay clearly showed a dose-dependent increase in the percentage of apoptotic cells for all four tumor cell lines. This indicates that PJ34 eradicated tumor cells by apoptosis, though previous studies demonstrated conflicted results.

The scratch wound assay results displayed that there was a dose-dependent inhibition of wound closure by PJ34. In literature, PJ34 is found to both inhibit and accelerate wound closure. The delay in wound closing time found in this thesis could be caused by the increase of PARP1 found by WB. The WB results showed that while PARP1 was inhibited for the H1_DL2 cell line, the amount of PARP1 generally increased after treatment with PJ34. The upregulation of PARP1 might be due to an overcompensating mechanism in the treated cells.

In addition, the amount of cleaved PARP1 also increased after drug treatment compared to the untreated controls.

Three dimensional cell cultures are believed to more accurately betray the complexity of the *in vivo* tumor microenvironment. Therefore, the growth inhibition of the tumor spheroids by PJ34 is an important finding in this current thesis. However, the *in vivo* experiment showed that the drug did not have any effect on the tumor size. As PJ34 has been found to inhibit tumor cell growth *in vivo* in previous studies, pretreatment with PJ34 before tumor cell injection or higher drug dosages may prove effective. The WB done on the *in vivo* tumors demonstrated an increase in the amount of both PARP1 and cleaved PARP1 in the tumors treated with drug compared to the control tumors. The increased PARP1 expression may be due to the same overcompensation mechanism as described for our *in vitro* result.

In conclusion, we found that PJ34 effectively inhibits metastatic melanoma cell lines *in vitro*. However, it also seems that PJ34 is not a specific PARP1 inhibitor, but my act on other pathways like the PI3K-Akt pathway.

5.9 Future Aspects

To obtain a more detailed image of the effect of PJ34 on metastatic melanoma, several of the experiments should be repeated or expanded. The experiments should include a broader range of drug doses as well as more diverse lengths of treatment. Exploring other melanoma cell lines may also be valued.

The effect of PJ34 on healthy tissue should be investigated further. The SV80 cell line was tested for cell viability after PJ34 treatment. This cell line, as well as other normal cell lines (endothelial cells, fibroblasts, brain astrocytes, etc.) could be investigated further with similar *in vitro* assays as used.

The effect of PJ34 on the amount of PAR, and caspase 3 (for the cleavage of PARP) by WB should be investigated further. Though caspase 3 was tested in this thesis, no clear bands from the WB assay could be retrieved (data not shown). However, caspase 3 should be obtained from several different vendors, in order to find the best quality antibody.

In addition, there is of course a need for much more detailed investigation of the effect of PJ34 on PARP1. Several other drug doses should be tested as well as shortening or extending the treatment time before preparing the cell lysate for WB. Most important, however, is the need for a WB investigation on the amount of PARP1 in apoptotic cells after PJ34 treatment. In addition, further investigations on PJ34 and its effect on the PI3K-Akt pathway, e.g. WB on mTOR should be performed.

A new *in vivo* experiment should be performed. The drug doses should be increased and injected daily. In addition, as Inbar-Rozensal and colleagues results shows, PJ34 may be utilized as a preventative form of treatment, as discussed in subchapter 5.7 (83). If positive effects of the drug are established, other animal tumor models could also be tried out. As an example, injecting tumor cells in the left cardiac ventricle would be one way to better examine the drug effect on metastatic melanoma, including brain metastasis.

Reference List:

1. Crosby T, Fish R, Coles B, Mason MD. Systemic treatments for metastatic cutaneous melanoma. The Cochrane database of systematic reviews. 2000(2):Cd001215.
2. Burge S, Wallis D. Oxford Handbook of Medical Dermatology. First Edition ed. United States: Oxford University Press; 2011, p. 12, 314, 322-323 and 330.
3. Jerant AF, Johnson JT, Sheridan CD, Caffrey TJ. Early detection and treatment of skin cancer. American family physician. 2000;62(2):357-68, 75-6, 81-2.
4. Dunki-Jacobs EM, Callender GG, McMasters KM. Current management of melanoma. Current problems in surgery. 2013;50(8):351-82.
5. DermaCompare. Skin Cancer [cited 2016-12-01]. Available from: http://www.dermacompare.com/skin-cancer/.
6. Oslo: Cancer Registry of Norway. Cancer in Norway 2013 - Cancer incidence, mortality, survival and prevalance in Norway p. 92. Larsen IK, editor.
7. Thorsen F, Fite B, Mahakian LM, Seo JW, Qin S, Harrison V, et al. Multimodal imaging enables early detection and characterization of changes in tumor permeability of brain metastases. Journal of controlled release : official journal of the Controlled Release Society. 2013;172(3):812-22.
8. Kreft Registeret Institutt for populasjonsbasert kreftforskning. Føflekkreft [updated 2014-09-26; cited 2015-02-28]. Available from: http://www.kreftregisteret.no/no/Generelt/Fakta-om-kreft-test/Foflekkreft/.
9. Oslo: Cancer Registry of Norway. Cancer in Norway 2013 - Cancer incidence, mortality, survival and prevalance in Norway p. 76-77. Larsen IK, editor.
10. Bhatia S, Tykodi SS, Thompson JA. Treatment of metastatic melanoma: an overview. Oncology. 2009;23(6):488-96.
11. Pecorino L. Molecular Biology of Cancer, p. 29-31. Third Edition ed. United Kingdom: Oxford University Press; 2012.
12. Bandarchi B, Ma L, Navab R, Seth A, Rasty G. From melanocyte to metastatic malignant melanoma. Dermatology research and practice. 2010;2010.
13. Manga P, Hoek KS, Davids LM, Leachman SA. From melanocyte to malignant metastatic melanoma. Dermatology research and practice. 2010;2010.
14. Bandarchi B, Jabbari CA, Vedadi A, Navab R. Molecular biology of normal melanocytes and melanoma cells. Journal of clinical pathology. 2013;66(8):644-8.
15. World Health Organization. Health effects of UV radiation [cited 2015-02-28]. Available from: http://www.who.int/uv/health/uv_health2/en/index1.html.
16. National Cancer Institute. Melanoma Treatment (PDQ®)–Patient Version [updated 2016-07-22],[cited 2016-11-30]. Available from: https://www.cancer.gov/types/skin/patient/melanoma-treatment-pdq#section/all.
17. Hawryluk EB, Tsao H. Melanoma: clinical features and genomic insights. Cold Spring Harbor perspectives in medicine. 2014;4(9):a015388.
18. Chin L, Garraway LA, Fisher DE. Malignant melanoma: genetics and therapeutics in the genomic era. Genes & development. 2006;20(16):2149-82.
19. McLaughlin CC, Wu XC, Jemal A, Martin HJ, Roche LM, Chen VW. Incidence of noncutaneous melanomas in the U.S. Cancer. 2005;103(5):1000-7.
20. Mooi W, Krausz T. Pathology of Melanocytic Disorders 2. edition, p. 399 ed. London, UK: Hodder Headline Group; 2007.
21. Agar N, Young AR. Melanogenesis: a photoprotective response to DNA damage? Mutation research. 2005;571(1-2):121-32.

22. National Cancer Institute. Genetics of Skin Cancer (PDQ®)–Health Professional Version [updated 2016-10-19],[cited 2016-11-19]. Available from: https://www.cancer.gov/types/skin/hp/skin-genetics-pdq.
23. Kanzler MH, Mraz-Gernhard S. Primary cutaneous malignant melanoma and its precursor lesions: diagnostic and therapeutic overview. Journal of the American Academy of Dermatology. 2001;45(2):260-76.
24. Lovly C, Pao W, Sosman J. Molecular Profiling of Melanoma [updated 2016-01-26][cited 2016-11-22]. Available from: My cancer genome: https://www.mycancergenome.org/content/disease/melanoma/.
25. Besaratinia A, Tommasi S. Epigenetics of human melanoma: promises and challenges. Journal of molecular cell biology. 2014;6(5):356-67.
26. Daphu I, Horn S, Stieber D, Varughese JK, Spriet E, Dale HA, et al. In vitro treatment of melanoma brain metastasis by simultaneously targeting the MAPK and PI3K signaling pathways. International journal of molecular sciences. 2014;15(5):8773-94.
27. Rehman FL, Lord CJ, Ashworth A. The promise of combining inhibition of PI3K and PARP as cancer therapy. Cancer discovery. 2012;2(11):982-4.
28. Klein HL. The consequences of Rad51 overexpression for normal and tumor cells. DNA repair. 2008;7(5):686-93.
29. Natinal Cancer Instistute. Stages of Melanoma [updated 2016-07-22][cited 2016-11-23]. Available from: https://www.cancer.gov/types/skin/patient/melanoma-treatment-pdq#section/_96.
30. Tidy C. Malignant Melanoma of Skin [updated 2015-8-18][cited 2016-11-23]. Available from: http://patient.info/doctor/malignant-melanoma-of-skin.
31. Geller AC, Swetter S. Screening and early detection of melanoma [updated 2016-10-18][cited 2016-11-23]. Available from: https://www.uptodate.com/contents/screening-and-early-detection-of-melanoma#H15.
32. Busch K. Stages of Melanoma [cited 2016-11-23]. Available from: http://dyersburgskinandallergyclinic.com/?p=311.
33. Geiger TR, Peeper DS. Metastasis mechanisms. Biochimica et biophysica acta. 2009;1796(2):293-308.
34. Tsai JH, Yang J. Epithelial-mesenchymal plasticity in carcinoma metastasis. Genes & development. 2013;27(20):2192-206.
35. Hanahan D, Weinberg RA. Hallmarks of Cancer: The Next Generation. Cell. 2011;144(5):646-74.
36. Nathoo N, Chahlavi A, Barnett GH, Toms SA. Pathobiology of brain metastases. Journal of clinical pathology. 2005;58(3):237-42.
37. Nygaard V, Prasmickaite L, Vasiliauskaite K, Clancy T, Hovig E. Melanoma brain colonization involves the emergence of a brain-adaptive phenotype. Oncoscience. 2014;1(1):82-94.
38. Leong SP, Mihm MC, Jr., Murphy GF, Hoon DS, Kashani-Sabet M, Agarwala SS, et al. Progression of cutaneous melanoma: implications for treatment. Clinical & experimental metastasis. 2012;29(7):775-96.
39. Tosoni A, Ermani M, Brandes AA. The pathogenesis and treatment of brain metastases: a comprehensive review. Critical reviews in oncology/hematology. 2004;52(3):199-215.
40. Advances in Nuclear Oncology: Diagnosis and Theraphy p. 24. 2015-01-27 ed. Emilio Bombardieri JB, Giovanni Lucignani, Otmar Schober, editor. Florida, USA: Taylor and Francis Group; 2007.
41. National Cancer Institute. General Information About Adult Brain Tumors [updated 2015-02-25], [cited 2015-03-02]. Available from: http://www.cancer.gov/cancertopics/pdq/treatment/adultbrain/HealthProfessional/page1.
42. Patchell RA. The management of brain metastases. Cancer treatment reviews. 2003;29(6):533-40.

43. Pardridge WM. The blood-brain barrier: bottleneck in brain drug development. NeuroRx : the journal of the American Society for Experimental NeuroTherapeutics. 2005;2(1):3-14.
44. McWilliams RR, Rao RD, Buckner JC, Link MJ, Markovic S, Brown PD. Melanoma-induced brain metastases. Expert review of anticancer therapy. 2008;8(5):743-55.
45. Fonkem E, Uhlmann EJ, Floyd SR, Mahadevan A, Kasper E, Eton O, et al. Melanoma brain metastasis: overview of current management and emerging targeted therapies. Expert review of neurotherapeutics. 2012;12(10):1207-15.
46. Rodriguez MI, Peralta-Leal A, O'Valle F, Rodriguez-Vargas JM, Gonzalez-Flores A, Majuelos-Melguizo J, et al. PARP-1 regulates metastatic melanoma through modulation of vimentin-induced malignant transformation. PLoS genetics. 2013;9(6):e1003531.
47. Ossovskaya V, Koo IC, Kaldjian EP, Alvares C, Sherman BM. Upregulation of Poly (ADP-Ribose) Polymerase-1 (PARP1) in Triple-Negative Breast Cancer and Other Primary Human Tumor Types. Genes & cancer. 2010;1(8):812-21.
48. Brown JS, Kaye SB, Yap TA. PARP inhibitors: the race is on. British journal of cancer. 2016;114(7):713-5.
49. McPherson LA, Shen Y, Ford JM. Poly (ADP-ribose) polymerase inhibitor LT-626: Sensitivity correlates with MRE11 mutations and synergizes with platinums and irinotecan in colorectal cancer cells. Cancer letters. 2014;343(2):217-23.
50. Rouleau M, Patel A, Hendzel MJ, Kaufmann SH, Poirier GG. PARP inhibition: PARP1 and beyond. Nature reviews Cancer. 2010;10(4):293-301.
51. Javle M, Curtin NJ. The role of PARP in DNA repair and its therapeutic exploitation. British journal of cancer. 2011;105(8):1114-22.
52. Murai J, Huang SY, Das BB, Renaud A, Zhang Y, Doroshow JH, et al. Trapping of PARP1 and PARP2 by Clinical PARP Inhibitors. Cancer research. 2012;72(21):5588-99.
53. Ip LR, Poulogiannis G, Viciano FC, Sasaki J, Kofuji S, Spanswick VJ, et al. Loss of INPP4B causes a DNA repair defect through loss of BRCA1, ATM and ATR and can be targeted with PARP inhibitor treatment. Oncotarget. 2015;6(12):10548-62.
54. Drew Y, Ledermann J, Hall G, Rea D, Glasspool R, Highley M, et al. Phase 2 multicentre trial investigating intermittent and continuous dosing schedules of the poly(ADP-ribose) polymerase inhibitor rucaparib in germline BRCA mutation carriers with advanced ovarian and breast cancer. British journal of cancer. 2016;114(12):e21.
55. Xiong T, Wei H, Chen X, Xiao H. PJ34, a poly(ADP-ribose) polymerase (PARP) inhibitor, reverses melphalan-resistance and inhibits repair of DNA double-strand breaks by targeting the FA/BRCA pathway in multidrug resistant multiple myeloma cell line RPMI8226/R. International journal of oncology. 2015;46(1):223-32.
56. Helleday T, Bryant HE, Schultz N. Poly(ADP-ribose) polymerase (PARP-1) in homologous recombination and as a target for cancer therapy. Cell cycle (Georgetown, Tex). 2005;4(9):1176-8.
57. Huang SH, Xiong M, Chen XP, Xiao ZY, Zhao YF, Huang ZY. PJ34, an inhibitor of PARP-1, suppresses cell growth and enhances the suppressive effects of cisplatin in liver cancer cells. Oncology reports. 2008;20(3):567-72.
58. Gangopadhyay NN, Luketich JD, Opest A, Visus C, Meyer EM, Landreneau R, et al. Inhibition of poly(ADP-ribose) polymerase (PARP) induces apoptosis in lung cancer cell lines. Cancer investigation. 2011;29(9):608-16.
59. Santa Cruz Biotechnology. PARP Inhibitor VIII, PJ34 (CAS 344458-15-7) [cited 2015-03-02]. Available from: http://www.scbt.com/datasheet-204161-parp-inhibitor-viii-pj34.html.
60. Antolin AA, Jalencas X, Yelamos J, Mestres J. Identification of pim kinases as novel targets for PJ34 with confounding effects in PARP biology. ACS chemical biology. 2012;7(12):1962-7.
61. Castiel A, Visochek L, Mittelman L, Dantzer F, Izraeli S, Cohen-Armon M. A phenanthrene derived PARP inhibitor is an extra-centrosomes de-clustering agent exclusively eradicating human cancer cells. BMC cancer. 2011;11:412.

62. Castiel A, Visochek L, Mittelman L, Zilberstein Y, Dantzer F, Izraeli S, et al. Cell death associated with abnormal mitosis observed by confocal imaging in live cancer cells. Journal of visualized experiments : JoVE. 2013(78):e50568.
63. Bai XT, Moles R, Chaib-Mezrag H, Nicot C. Small PARP inhibitor PJ-34 induces cell cycle arrest and apoptosis of adult T-cell leukemia cells. Journal of hematology & oncology. 2015;8:117.
64. Teng F, Beray-Berthat V, Coqueran B, Lesbats C, Kuntz M, Palmier B, et al. Prevention of rt-PA induced blood-brain barrier component degradation by the poly(ADP-ribose)polymerase inhibitor PJ34 after ischemic stroke in mice. Experimental neurology. 2013;248:416-28.
65. Kimlin LC, Casagrande G, Virador VM. In vitro three-dimensional (3D) models in cancer research: an update. Molecular carcinogenesis. 2013;52(3):167-82.
66. Baker BM, Chen CS. Deconstructing the third dimension: how 3D culture microenvironments alter cellular cues. Journal of cell science. 2012;125(Pt 13):3015-24.
67. Pampaloni F, Reynaud EG, Stelzer EH. The third dimension bridges the gap between cell culture and live tissue. Nature reviews Molecular cell biology. 2007;8(10):839-45.
68. O'Brien J, Wilson I, Orton T, Pognan F. Investigation of the Alamar Blue (resazurin) fluorescent dye for the assessment of mammalian cell cytotoxicity. European journal of biochemistry. 2000;267(17):5421-6.
69. Al-Nasiry S, Geusens N, Hanssens M, Luyten C, Pijnenborg R. The use of Alamar Blue assay for quantitative analysis of viability, migration and invasion of choriocarcinoma cells. Human reproduction (Oxford, England). 2007;22(5):1304-9.
70. Ormerod MG. Flow Cytometry - A Basic Introduction 2008 [cited 2016-11-24]. Available from: http://flowbook.denovosoftware.com/.
71. Abcam. Annexin V detection protocol for apoptosis [cited 2016-11-24]. Available from: http://www.abcam.com/protocols/annexin-v-detection-protocol-for-apoptosis.
72. Koopman G, Reutelingsperger CP, Kuijten GA, Keehnen RM, Pals ST, van Oers MH. Annexin V for flow cytometric detection of phosphatidylserine expression on B cells undergoing apoptosis. Blood. 1994;84(5):1415-20.
73. Liu ZQ, Mahmood T, Yang PC. Western blot: technique, theory and trouble shooting. North American journal of medical sciences. 2014;6(3):160.
74. Wang J, Daphu I, Pedersen PH, Miletic H, Hovland R, Mork S, et al. A novel brain metastases model developed in immunodeficient rats closely mimics the growth of metastatic brain tumours in patients. Neuropathology and applied neurobiology. 2011;37(2):189-205.
75. Prasmickaite L, Skrbo N, Hoifodt HK, Suo Z, Engebraten O, Gullestad HP, et al. Human malignant melanoma harbours a large fraction of highly clonogenic cells that do not express markers associated with cancer stem cells. Pigment cell & melanoma research. 2010;23(3):449-51.
76. Abcam. Transfer and staining of proteins in western blot [cited 2016-10-15]. Available from: http://www.abcam.com/protocols/transfer-and-staining-of-proteins-in-western-blot.
77. Vinci M, Gowan S, Boxall F, Patterson L, Zimmermann M, Court W, et al. Advances in establishment and analysis of three-dimensional tumor spheroid-based functional assays for target validation and drug evaluation. BMC biology. 2012;10:29.
78. Oltersdorf T, Elmore SW, Shoemaker AR, Armstrong RC, Augeri DJ, Belli BA, et al. An inhibitor of Bcl-2 family proteins induces regression of solid tumours. Nature. 2005;435(7042):677-81.
79. Sundstrom T, Daphu I, Wendelbo I, Hodneland E, Lundervold A, Immervoll H, et al. Automated tracking of nanoparticle-labeled melanoma cells improves the predictive power of a brain metastasis model. Cancer research. 2013;73(8):2445-56.
80. Pardridge WM. Drug transport across the blood-brain barrier. Journal of cerebral blood flow and metabolism : official journal of the International Society of Cerebral Blood Flow and Metabolism. 2012;32(11):1959-72.
81. Horibata S, Vo TV, Subramanian V, Thompson PR, Coonrod SA. Utilization of the Soft Agar Colony Formation Assay to Identify Inhibitors of Tumorigenicity in Breast Cancer Cells. Journal of visualized experiments : JoVE. 2015(99):e52727.

82. Chevanne M, Zampieri M, Caldini R, Rizzo A, Ciccarone F, Catizone A, et al. Inhibition of PARP activity by PJ-34 leads to growth impairment and cell death associated with aberrant mitotic pattern and nucleolar actin accumulation in M14 melanoma cell line. Journal of cellular physiology. 2010;222(2):401-10.
83. Inbar-Rozensal D, Castiel A, Visochek L, Castel D, Dantzer F, Izraeli S, et al. A selective eradication of human nonhereditary breast cancer cells by phenanthridine-derived polyADP-ribose polymerase inhibitors. Breast cancer research : BCR. 2009;11(6):R78.
84. Xiong T, Chen X, Wei H, Xiao H. Influence of PJ34 on the genotoxicity induced by melphalan in human multiple myeloma cells. Archives of medical science : AMS. 2015;11(2):301-6.
85. Wang Z, Li Y, Lv S, Tian Y. Inhibition of proliferation and invasiveness of ovarian cancer C13* cells by a poly(ADP-ribose) polymerase inhibitor and the role of nuclear factor-kappaB. The Journal of international medical research. 2013;41(5):1577-85.
86. Cooper G. The Cell: A Molecular Approach. 2nd edition. The Eucaryotic Cell Cycle. Sunderland (MA), Sinauer Associates, editors. 2000.
87. Madison DL, Stauffer D, Lundblad JR. The PARP inhibitor PJ34 causes a PARP1-independent, p21 dependent mitotic arrest. DNA repair. 2011;10(10):1003-13.
88. Gaymes TJ, Shall S, MacPherson LJ, Twine NA, Lea NC, Farzaneh F, et al. Inhibitors of poly ADP-ribose polymerase (PARP) induce apoptosis of myeloid leukemic cells: potential for therapy of myeloid leukemia and myelodysplastic syndromes. Haematologica. 2009;94(5):638-46.
89. Acton QA. Melanomas: New Insights for the Healthcare Professional, page 148: ScholarlyEditions, Atlanta, Georgia; 2011.
90. El-Hamoly T, Hegedus C, Lakatos P, Kovacs K, Bai P, El-Ghazaly MA, et al. Activation of poly(ADP-ribose) polymerase-1 delays wound healing by regulating keratinocyte migration and production of inflammatory mediators. Molecular medicine (Cambridge, Mass). 2014;20:363-71.
91. Zhou X, Patel D, Sen S, Shanmugam V, Sidawy A, Mishra L, et al. Poly-ADP-ribose polymerase inhibition enhances ischemic and diabetic wound healing by promoting angiogenesis. Journal of vascular surgery. 2016.
92. A Textbook of Modern Toxicology, p. 219-220. Third edition ed. Hodgson E, editor. New Jersey, USA: A John While and sons, INC., publications; 2004.
93. D'Onofrio G, Tramontano F, Dorio AS, Muzi A, Maselli V, Fulgione D, et al. Poly(ADP-ribose) polymerase signaling of topoisomerase 1-dependent DNA damage in carcinoma cells. Biochemical pharmacology. 2011;81(2):194-202.
94. Davies AA, Masson JY, McIlwraith MJ, Stasiak AZ, Stasiak A, Venkitaraman AR, et al. Role of BRCA2 in control of the RAD51 recombination and DNA repair protein. Molecular cell. 2001;7(2):273-82.
95. Alagpulinsa DA, Ayyadevara S, Shmookler Reis RJ. A Small-Molecule Inhibitor of RAD51 Reduces Homologous Recombination and Sensitizes Multiple Myeloma Cells to Doxorubicin. Frontiers in oncology. 2014;4:289.
96. Wang S, Wang H, Davis BC, Liang J, Cui R, Chen SJ, et al. PARP1 inhibitors attenuate AKT phosphorylation via the upregulation of PHLPP1. Biochemical and biophysical research communications. 2011;412(2):379-84.
97. Vultur A, Villanueva J, Herlyn M. Targeting BRAF in advanced melanoma: a first step toward manageable disease. Clinical cancer research : an official journal of the American Association for Cancer Research. 2011;17(7):1658-63.
98. Szanto A, Hellebrand EE, Bognar Z, Tucsek Z, Szabo A, Gallyas F, Jr., et al. PARP-1 inhibition-induced activation of PI-3-kinase-Akt pathway promotes resistance to taxol. Biochemical pharmacology. 2009;77(8):1348-57.
99. Ho WY, Yeap SK, Ho CL, Rahim RA, Alitheen NB. Development of multicellular tumor spheroid (MCTS) culture from breast cancer cell and a high throughput screening method using the MTT assay. PloS one. 2012;7(9):e44640.

100. Kelm JM, Timmins NE, Brown CJ, Fussenegger M, Nielsen LK. Method for generation of homogeneous multicellular tumor spheroids applicable to a wide variety of cell types. Biotechnology and bioengineering. 2003;83(2):173-80.
101. Kim JB, Stein R, O'Hare MJ. Three-dimensional in vitro tissue culture models of breast cancer-- a review. Breast cancer research and treatment. 2004;85(3):281-91.
102. Sutherland RM. Cell and environment interactions in tumor microregions: the multicell spheroid model. Science (New York, NY). 1988;240(4849):177-84.
103. Fracasso G, Colombatti M. Effect of therapeutic macromolecules in spheroids. Critical reviews in oncology/hematology. 2000;36(2-3):159-78.
104. Minchinton AI, Tannock IF. Drug penetration in solid tumours. Nature reviews Cancer. 2006;6(8):583-92.